PLA2G2E-mediated lipid metabolism triggers brain-autonomous neural repair after ischemic stroke
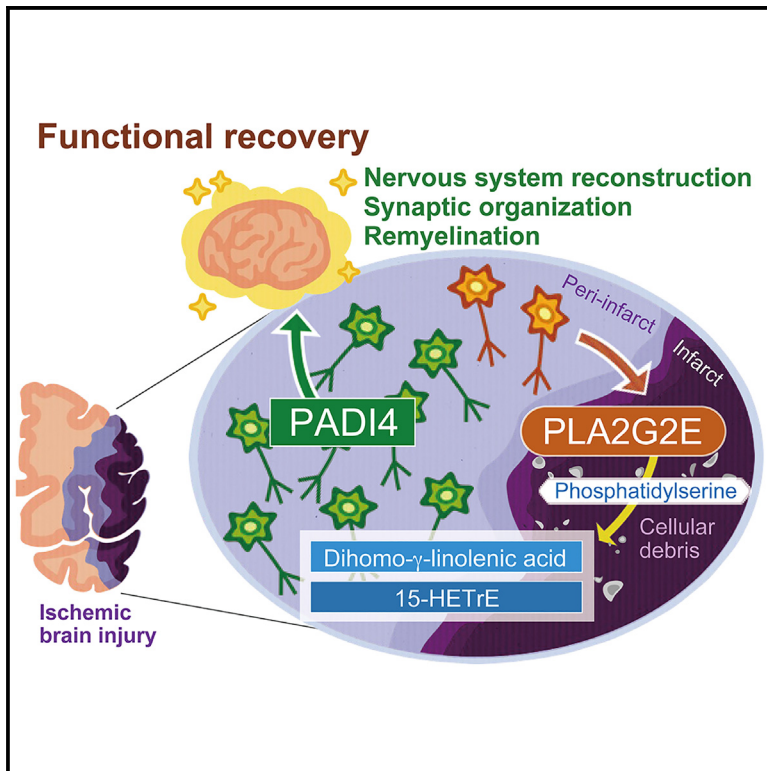
Graphical abstract

Highlights

- PLA2G2E generates DGLA and 15-HETrE to induce neuronal PADI4 for stroke recovery

- PADI4 is necessary for recovery-associated gene expression in peri-infarct neurons

- 15-HETrE administration promotes stroke recovery and neuronal PADI4 expression

Authors

Akari Nakamura, Seiichiro Sakai,
Yoshitaka Taketomi, ..., Hideya Kawaji,
Makoto Murakami, Takashi Shichita

Correspondence

shichita-tk@cmn.tmd.ac.jp

In brief

PLA2G2E from peri-infarct-surviving neurons metabolizes phosphatidylserine to DGLA and 15-HETrE, which triggers functional recovery after ischemic stroke. These reparative lipid mediators induce PADI4 in peri-infarct-surviving neurons to initiate neural repair-associated gene expression through histone citrullination, demonstrating brain-autonomous extensive repair capabilities through lipid metabolism.

CellPress

Article

PLA2G2E-mediated lipid metabolism triggers brain-autonomous neural repair after ischemic stroke

Akari Nakamura,[1,2,8,9] Seiichiro Sakai,[1,2,8,9] Yoshitaka Taketomi,[3] Jun Tsuyama,[1,2,8] Yoshimi Miki,[3] Yuichiro Hara,[4] Nobutaka Arai,[5] Yuki Sugiura,[6] Hideya Kawaji,[4] Makoto Murakami,[3] and Takashi Shichita[1,2,7,8,10,*]

[1]Stroke Renaissance Project, Tokyo Metropolitan Institute of Medical Science, Tokyo 156-8506, Japan
[2]Department of Neuroinflammation and Repair, Medical Research Institute, Tokyo Medical and Dental University (TMDU), Tokyo 113-8510, Japan
[3]Laboratory of Microenvironmental and Metabolic Health Science Center for Disease Biology and Integrative Medicine, Graduate School of Medicine, The University of Tokyo, Tokyo 113-8655, Japan
[4]Research Center for Genome & Medical Sciences, Tokyo Metropolitan Institute of Medical Science, Tokyo 156-8506, Japan
[5]Laboratory for Neuropathology, Tokyo Metropolitan Institute of Medical Science, Tokyo 156-8506, Japan
[6]Department of Biochemistry, Keio University School of Medicine, Tokyo 160-8582, Japan
[7]Department of Medicine and Clinical Science, Graduate School of Medical Sciences, Kyushu University, Fukuoka 812-8582, Japan
[8]Core Research for Evolutionary Medical Science and Technology (CREST), Japan Agency for Medical Research and Development (AMED), Tokyo 100-0004, Japan
[9]These authors contributed equally
[10]Lead contact
*Correspondence: shichita-tk@cmn.tmd.ac.jp
https://doi.org/10.1016/j.neuron.2023.06.024

SUMMARY

The brain is generally resistant to regeneration after damage. The cerebral endogenous mechanisms triggering brain self-recovery have remained unclarified to date. We here discovered that the secreted phospholipase PLA2G2E from peri-infarct neurons generated dihomo-γ-linolenic acid (DGLA) as necessary for triggering brain-autonomous neural repair after ischemic brain injury. *Pla2g2e* deficiency diminished the expression of peptidyl arginine deiminase 4 (Padi4), a global transcriptional regulator in peri-infarct neurons. Single-cell RNA sequencing (scRNA-seq) and epigenetic analysis demonstrated that neuronal PADI4 had the potential for the transcriptional activation of genes associated with recovery processes after ischemic stroke through histone citrullination. Among various DGLA metabolites, we identified 15-hydroxy-eicosatrienoic acid (15-HETrE) as the cerebral metabolite that induced PADI4 in peri-infarct-surviving neurons. Administration of 15-HETrE enhanced functional recovery after ischemic stroke. Thus, our research clarifies the promising potential of brain-autonomous neural repair triggered by the specialized lipids that initiate self-recovery processes after brain injury.

INTRODUCTION

In today's aging society, a large number of patients around the world suffer from neurological sequelae of brain tissue injury, including those brought about by major strokes.[1–3] Although the lost brain functions due to brain injury are often poorly recoverable, rehabilitation can improve patients' functional prognosis to some extent,[4–6] suggesting the existence of cerebral self-recovery mechanisms after injury.[7–9] Nervous system reconstruction, synapse organization, and remyelination are implicated in these recovery processes, which are induced by the various neurotrophins or factors regulating neurite projection or synaptogenesis around the injured region.[10–13] The neurons surrounding the injured region must not only survive despite injury stresses but also acquire reparative functions for efficient functional recovery.[14] The triggering molecular mechanisms that induce this broad range of neural repair after brain injury remain to be clarified.[15,16]

Necrotic cell death after injuries has broad effects; for example, the extracellular release of endogenous molecules called alarmin from dead cells is generally inflammatogenic.[17,18] We previously identified the peroxiredoxin (PRX) family proteins and DJ-1 (PARK7) released extracellularly from dead neurons as damage-associated molecular patterns (DAMPs) that directly activate infiltrating immune cells to produce inflammatory cytokines,[19,20] and their removal through scavenger receptors, macrophage scavenger receptor 1 (MSR1) or macrophage receptor with collagenous structure (MARCO), resolves cerebral

inflammation after ischemic brain injury.[21] Classically, various lipid mediators generated after tissue injuries are well known to regulate inflammation. Prostaglandins and leukotrienes, metabolites of ω6 arachidonic acid (AA; C20:4), are well-known pro-inflammatory lipid mediators.[22,23] By contrast, resolvins, neuroprotectin D1, and maresins metabolites of ω3 eicosapentaenoic acid (EPA; C20:5) or docosahexaenoic acid (DHA; C22:6) have recently been identified as pro-resolving lipid mediators.[23–25] These polyunsaturated fatty acids (PUFAs) and their metabolites are generated by the enzymatic activities of the various PLA2 subtypes from the phospholipids included in the cellular membrane or membranous debris after tissue injuries.[26–28] Among approximately fifty subtypes of PLA2, only PLA2G4A has been known to generate inflammatory lipid mediators in ischemic stroke,[22,23] whereas the functions of other PLA2 subtypes remain to be clarified.

Nevertheless, few cerebral endogenous molecules that trigger a broad range of neural repair after brain injury have been identified. These endogenous molecules are expected to be pro-survival and pro-reparative for the neurons around the injured region and to accelerate stroke recovery. In this study, we discovered the pivotal roles of the secreted phospholipase PLA2G2E from neurons that induced peptidyl arginine deiminase 4 (PADI4) expression to grant pro-survival and pro-reparative functions in peri-infarct neurons after ischemic brain injury. Neuronal PADI4 was important not only for preventing additional cell death and subsequent severe inflammation but also for inducing the peri-infarct neuronal populations bearing gene expression profiles associated with recovery processes after brain injury. PLA2G2E spatiotemporally generated the ω6 PUFA dihomo-γ-linolenic acid (DGLA; C20:3) and its metabolites, 15-hydroxy-eicosatrienoic acid (15-HETrE), in the ischemic brain to induce neuronal PADI4.

RESULTS

The level of DGLA metabolites increased in the post-ischemic brain

To identify the cerebral lipid metabolites necessary for triggering stroke recovery, we investigated the time-dependent changes of the fatty acid metabolites and lysophospholipids included in post-ischemic brain tissue by mass spectrometry. Principal component analysis of lipid composition revealed that the characteristics of these fatty acid metabolites and lysophospholipids changed along with the progression of ischemic stroke pathology (Figure 1A), although the level of various fatty acids, especially PUFAs (except AA), increased after stroke onset (Figure 1B). Consistently, the level of most AA metabolites decreased from day 3 to day 6 after stroke onset, whereas the level of EPA and DHA metabolites increased until day 6 after stroke onset (Figure 1C). It is noteworthy that the levels of some DGLA metabolites, whose function in the brain has not yet been clarified,[29–31] also increased until day 6 after stroke onset (Figure 1C). There was a considerable amount of DGLA metabolites in the brain compared with the metabolites of other fatty acids (Figure S1A). The level of lysophospholipids with a saturated fatty acyl chain mainly increased after stroke onset (Figures 1D and S1B), indicating the pivotal roles of some

PLA2s in ischemic stroke pathologies that liberate these lysophospholipids and PUFAs from membranous phospholipids.[26]

PLA2G2E plays an essential role in functional recovery after ischemic stroke

Therefore, we investigated the time-dependent expression profiles of various enzymes belonging to the PLA2 superfamily after ischemic stroke. Among the members of the cytosolic (cPLA2) or secreted PLA2 (sPLA2) family, the mRNA expression level of *Pla2g2e*, encoding group IIE sPLA2 with unknown function, increased markedly after stroke onset (Figure 2A) compared with *Pla2g4a*, which was reported to promote ischemic brain injury,[22] and *Pla2g4e* and *Pla2g5* markedly decreased (Figure 2A). To identify the important PLA2 subtype for functional recovery after ischemic stroke, we then focused on *Pla2g2e*, *Pla2g4e*, and *Pla2g5*, in addition to *Pla2g10* and *Pla2g12a*, which potentially regulate inflammation.[28,32] Using mice that lacked each of these genes, we discovered that the severe neurological deficits in *Pla2g2e*-deficient mice were sustained until day 7 after stroke onset (Figure 2B). *Pla2g2e* deficiency significantly enlarged the infarct volume after ischemic stroke compared with wild-type (WT) mice or mice lacking other PLA2 subtypes (Figure 2C; Table S1), suggesting the essential role of PLA2G2E in functional recovery after ischemic brain injury.

Pla2g2e mRNA expression was detectable on day 1 and reached a remarkable level on day 3 in the ischemic brain (Figure 2D), which was almost completely dependent on the myeloid differentiation factor 88-(MYD88) and TIR domain-containing adaptor protein inducing interferon beta- (TRIF)-dependent signaling pathway, one of the major inflammatory and neuroprotective signaling cascades activated by necrotic cell death after ischemic brain injury[33,34] (Figure 2E). PLA2G2E expression was confirmed by immunohistochemistry in the peri-infarct neurons but was not observed in the sham-operated normal brain or the *Pla2g2e*-deficient peri-infarct region (Figure 2F). *Pla2g2e* deficiency significantly enlarged infarct volume on day 4 but not on day 1 after stroke onset compared with WT mice (Figure 2G), suggesting that PLA2G2E had neuroprotective function from days 1 to 4. Microarray analysis of mRNA expression in ischemic brain tissue on day 3 after stroke onset revealed that *Pla2g2e* deficiency enhanced the gene expression implicated in inflammatory responses (Figures 2H and S2A). Indeed, a significantly increased expression of inflammatory cytokines in the immune cell-enriched population collected from post-ischemic day 3 brain was observed in *Pla2g2e*-deficient mice (Figure 2I). By contrast, microarray analysis indicated that *Pla2g2e* deficiency impaired the expression of genes related to the development of the nervous system and synaptic modulation, such as *Ngfr*, *Aplnr*, or *Gal* genes, which were mainly expressed in neurons[35] (Figures 2J and S2B)—this suggests the pivotal pro-survival and pro-reparative roles of PLA2G2E in the peri-infarct neurons to enhance stroke recovery. These phenomena may be explained by the loss of *Padi4*, a global transcriptional regulator[36–39] that was the most decreased gene in *Pla2g2e*-deficient ischemic brain tissue (Figure 2J). In this context, we investigated the function of *Padi4* in ischemic brain injury.
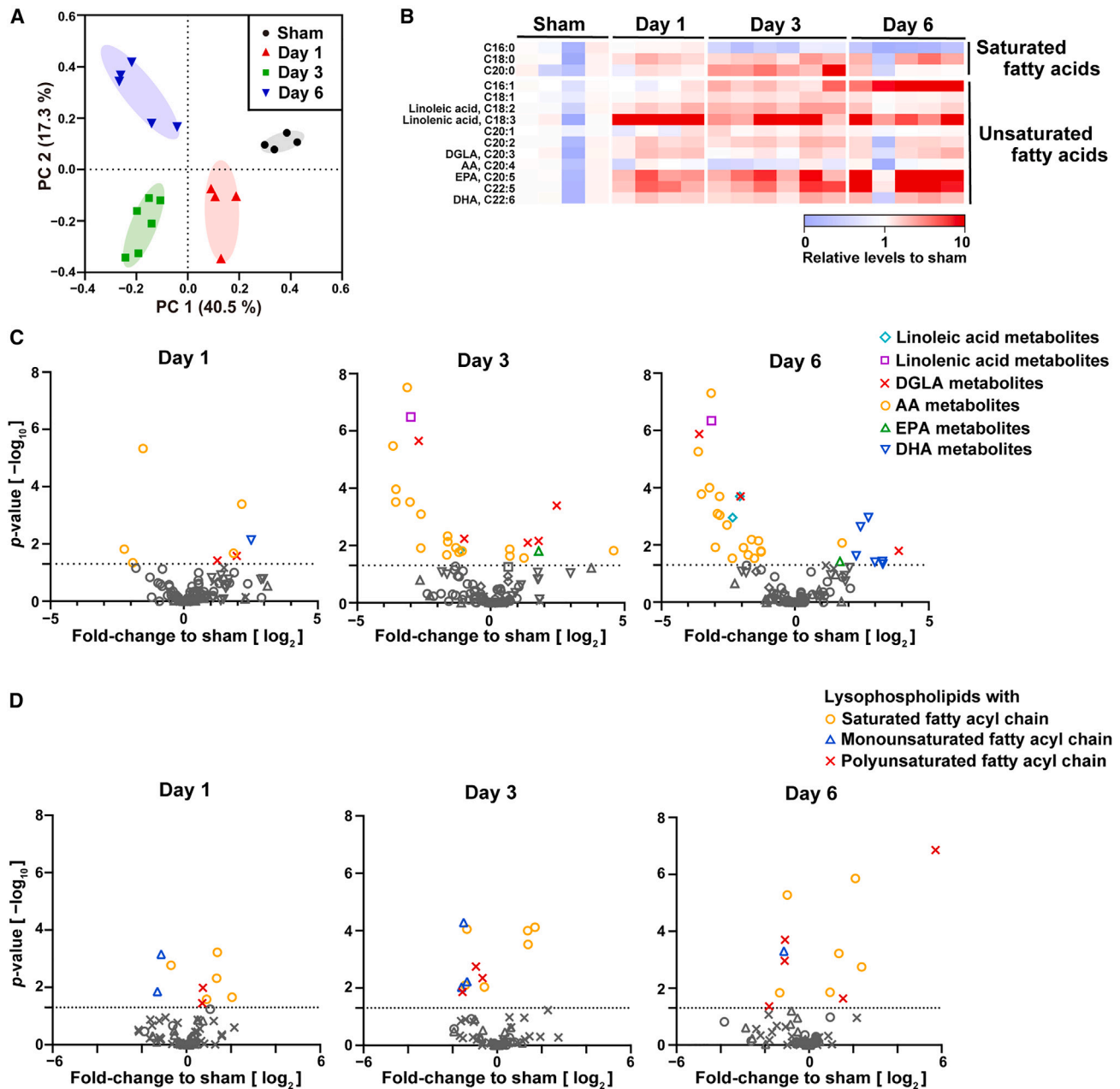
Figure 1. The time-dependent changes of glycerophospholipid metabolites in brain after ischemic injury
(A) PCA analysis of lipid levels with significant changes before and after ischemic stroke.
(B) Heatmap showing the levels of fatty acids in the ischemic brain tissue relative to the sham-operated brain.
(C and D) The time-dependent changes of unsaturated fatty acid metabolites (C) and lysophospholipids (D) after ischemic stroke. Fold changes relative to the sham-operated brain are shown. The dashed line indicates $p = 0.05$ vs. the sham-operated brain (one-way ANOVA with Dunnett's test).

Neuronal PADI4 prevents infarct growth and severe sterile inflammation

We confirmed the minimal expression of *Padi4* mRNA in the ischemic brain tissue of *Pla2g2e*-deficient mice on day 4 after stroke onset (Figure 3A). *Padi4* was not expressed in normal or day 1 post-ischemic brain tissue, but its expression was apparent on day 4 after stroke onset (Figure 3B). *Padi4* is known to regulate inflammation in rheumatoid arthritis through the in-

duction of neutrophil extracellular traps.[38] Although the infiltrating neutrophils and macrophages expressed PADI4 in the infarct area,[40] we discovered that PADI4 expression was also observed in peri-infarct-surviving neurons on day 4 after stroke onset but not in normal brain tissue or the excitatory and inhibitory neuron-specific *Padi4*-deficient peri-infarct region (Figure 3C). PADI4 expression was already detectable beginning on day 2 after ischemic stroke onset in peri-infarct neurons
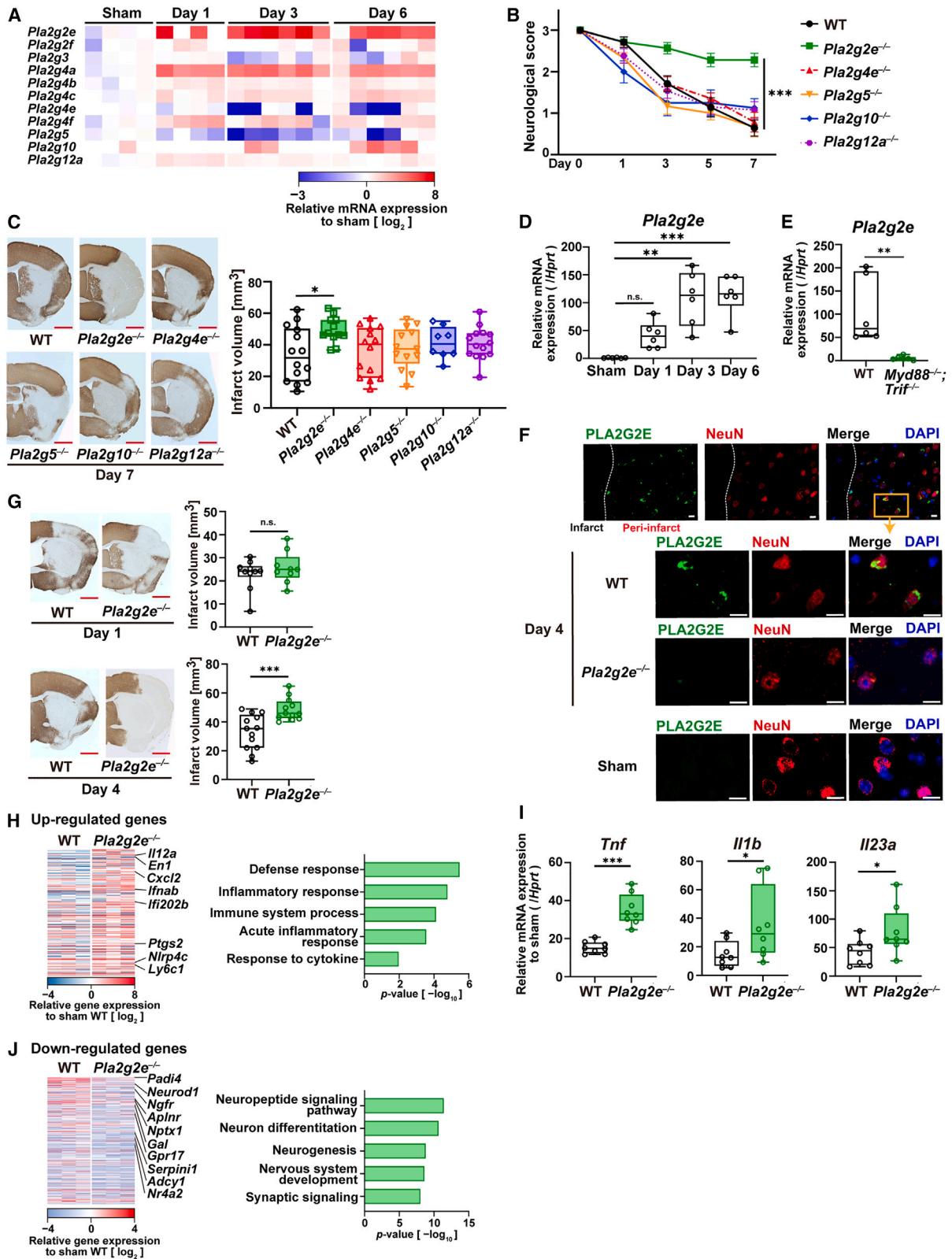
(Figures S3A and S3B), indicating PLA2G2E-induced PADI4 expression in peri-infarct neurons.

Next, we investigated if PADI4 expression was important for functional recovery after ischemic stroke. Since most of the PADI4-positive peri-infarct cells were either CAMKII-positive excitatory neurons or GAD67-positive inhibitory neurons (Figure 3D), we examined *Vglut1-Cre*; *Vgat-Cre*; *Padi4*flox/flox mice to investigate the neuronal PADI4 function in ischemic brain injury. *Padi4* deficiency in neurons impaired functional recovery after stroke, although the neurological deficits of *Padi4*flox/flox or *Lysm-Cre*; *Padi4*flox/flox mice were considerably improved by day 7 after stroke onset (Figure 3E). *Padi4* expression in the peri-infarct neurons promoted the survival of neuronal cells against brain ischemia, given that *Padi4* deficiency in neurons enlarged the infarct volume compared with *Padi4*flox/flox or *Lysm-Cre*; *Padi4*flox/flox mice on day 7 after stroke onset (Figure 3F; Table S2). Indeed, the number of TUNEL-positive dead neurons in the infarct boundary zone increased with *Padi4* deficiency in neurons on day 4 after stroke onset (Figure 3G). This exacerbated neuronal cell death resulted in an increased amount of neuronal inflammatogenic DAMPs, such as DJ-1 and PRX5, in the extracellular space of the TUNEL-positive infarct region as previously described[19,20] (Figure 3H). *Padi4* deficiency in neurons did not change the expression of MSR1 and MARCO, important scavenger receptors for the clearance of DAMPs in infiltrating macrophage[21] (Figure 3I), but significantly increased the expression of inflammatory cytokines in infiltrating immune cells on day 4 after stroke onset (Figure 3J). Thus, these results indicated that the exacerbated neuronal cell death and subsequent severe inflammation observed in *Pla2g2e*-deficient mice could be explained by the loss of *Padi4* in peri-infarct neurons.

Peri-infarct neurons express PLA2G2E and Padi4 in stroke patients

To investigate the consistency of our findings between murine and human brains with ischemic stroke, we examined the expression of PLA2G2E and PADI4 in the surviving neurons around the infarct region of stroke patients (Table S3). The immunohistochemistry of human brain tissues revealed the expression of PLA2G2E in the peri-infarct neurons of ischemic stroke patients but not in the neurons of normal brain regions of ischemic stroke patients or control patients without ischemic

stroke (Figures 4A and 4B). PADI4 expression was also observed in the peri-infarct neurons of stroke patients but not in the neurons within the normal brain regions of control patients or ischemic stroke patients (Figures 4C and 4D). Since the *Pla2g2e* mRNA expression increased from day 1 to day 3 but *Padi4* expression was apparent on day 4 after stroke onset in the murine ischemic brain (Figures 2D and 3B), we investigated the number of PLA2G2E- or PADI4-positive neurons by dividing stroke brain samples into two groups, 2–3 days and 4–8 days after the onset of ischemic stroke (Figures 4B and 4D). The number of PLA2G2E-positive neurons around the infarct region significantly increased even on days 2–3 after stroke onset (Figure 4B), but with a delay to PLA2G2E expression, the number of PADI4-positive neurons around infarcts increased on days 4–8 after stroke onset (Figure 4D). These results indicate that a similar neuronal PLA2G2E-PADI4 pathway works in the human brain after ischemic stroke as observed in the murine model of ischemic stroke.

Neuronal PADI4 is necessary for recovery processes after brain injury

PADI4 is well known as a global transcriptional regulator necessary for the pluripotency of stem cells through the citrullination of histones and various intracellular proteins,[36–38] but its function in neurons remains to be clarified. We therefore investigated whether neuronal PADI4 is necessary for the gene expression profiles associated with recovery processes after brain injury. By applying the neuronal cell-sorting technique established previously,[41] we successfully isolated glutamatergic neurons from the peri-infarct region, which was confirmed by single-cell RNA sequencing (scRNA-seq) or fluorescence-activated cell sorting (FACS) analysis using glutamatergic neuron-specific reporter mice (Figure S4).

We prepared and sequenced scRNA-seq libraries from the sham-operated brain tissue and day 4 post-ischemic brain tissue of *Padi4*flox/flox and *Vglut1-Cre*; *Vgat-Cre*; *Padi4*flox/flox mice. Through the integration analysis of the scRNA-seq data of these samples, we identified the cell clusters of *Snap25*- and *Slc17a7*-positive glutamatergic neurons, as shown in uniform manifold approximation and projection (UMAP) (Figure 5A). We found a comparable cellular composition among the sham-operated and day 4 post-ischemic brains (Figure 5B), whereas

---

Figure 2. PLA2G2E played pivotal roles in functional recovery after ischemic brain injury

(A) The relative mRNA expression levels of PLA2 subtypes in the ischemic brain tissue compared with the sham-operated brain.

(B and C) (B) Neurological scores after stroke onset and (C) infarct volume on day 7 in each type of mice (n = 14 for WT, 12 for *Pla2g2e*−/−, 14 for *Pla2g4e*−/−, 13 for *Pla2g5*−/−, 8 for *Pla2g10*−/−, and 14 for *Pla2g12a*−/− mice). Scale bars, 1 mm.

(D) Quantification of *Pla2g2e* mRNA in brain tissue before and after ischemic stroke onset (n = 6 for each sample).

(E) Comparison of *Pla2g2e* mRNA expression levels in day 3 post-ischemic brain tissue between WT and *Myd88*−/−/*Trif*−/− mice (n = 6 for each sample).

(F) Immunohistochemistry of PLA2G2E and NeuN in the sham-operated brain tissue or peri-infarct region on day 4. Scale bars, 10 μm.

(G) Infarct volume on days 1 and 4 (n = 10 for WT, 9 for *Pla2g2e*−/− mice on day 1, n = 13 for WT, 12 for *Pla2g2e*−/− mice on day 4). Scale bars, 1 mm.

(H) The relative mRNA levels to the sham-operated brain increased in *Pla2g2e*−/− compared with WT ischemic brain tissue (left). Gene ontologies enriched in the gene list of the left are shown (right).

(I) The relative mRNA levels of inflammatory cytokines in the immune cell-enriched population collected from day 3 post-ischemic brain compared with the sham-operated brain (n = 8 for WT, 8 for *Pla2g2e*−/− mice).

(J) The relative mRNA levels decreased in *Pla2g2e*−/− compared with WT ischemic brain tissue (left) and enriched gene ontologies (right).

*p < 0.05, **p < 0.01, ***p < 0.001 vs. WT mice (B–E, G, and I) (two-way ANOVA with Tukey's test, B; one-way ANOVA with Dunnett's test, C; Kruskal-Wallis test with Dunn's test, D; Mann-Whitney U test, E; or two-sided Student's t test, G and I). n.s.: not significant. Error bars represent the mean ± standard error of the mean (SEM).
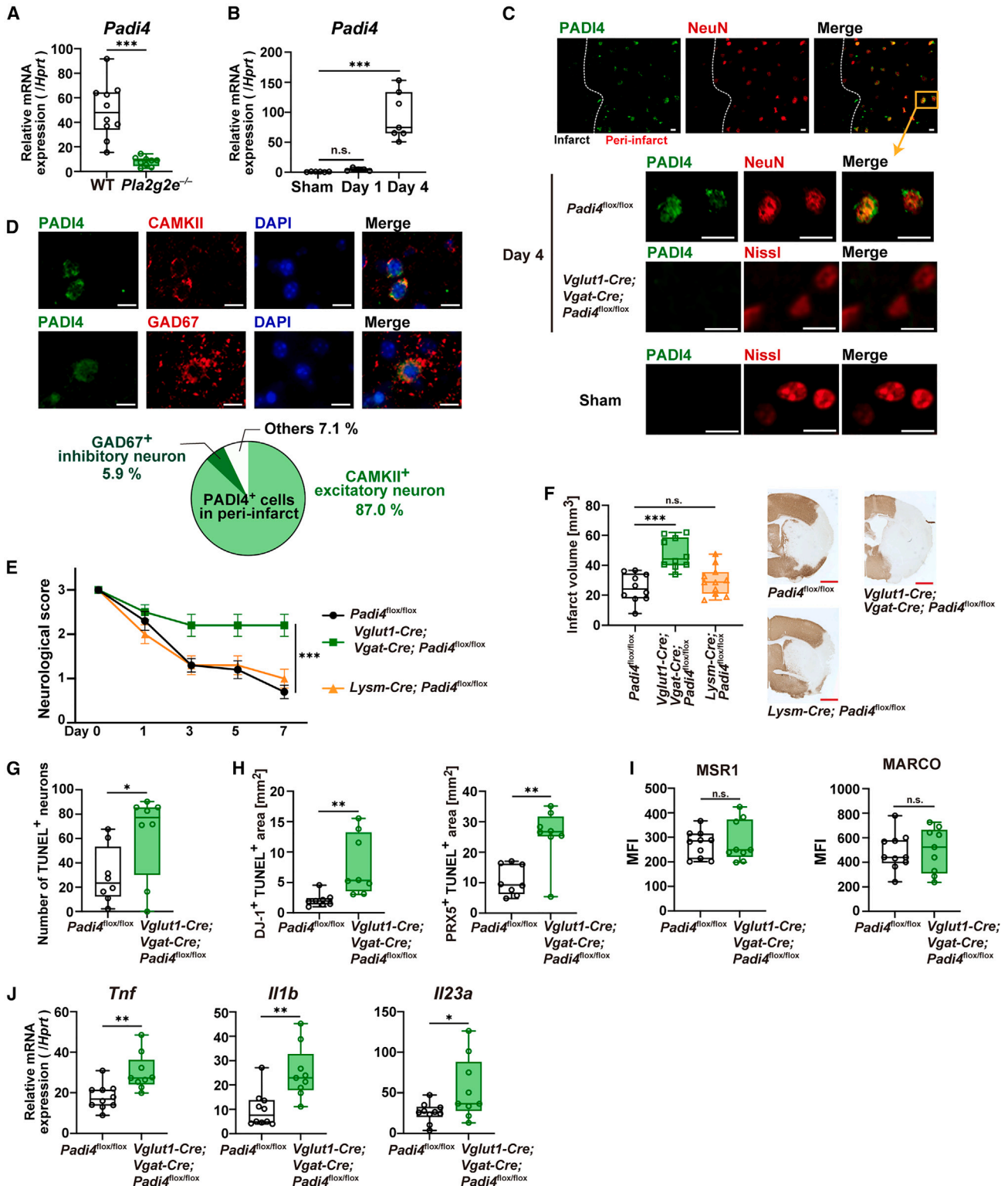
Figure 3. *Padi4* **deficiency in neurons with impaired functional recovery after ischemic brain injury**

(A and B) *Padi4* mRNA expression levels in day 3 post-ischemic brain tissue (A) and at each time point (B) relative to the sham-operated brain (n = 10 for WT and 9 for *Pla2g2e*^{−/−} mice, A; n = 6 for sham, 5 for day 1, and 7 for day 4, B).

(C and D) Immunohistochemistry of PADI4 and NeuN (C) or CAMKII and GAD67 (D) in the peri-infarct region on day 4. Scale bars, 10 μm.
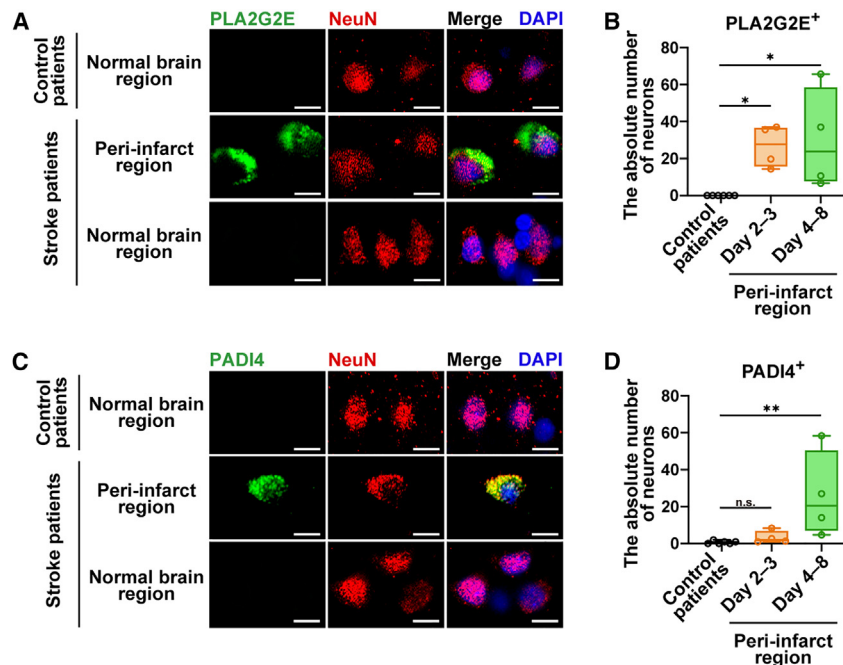
(legend continued on next page)

a larger amount of unspliced transcripts were observed in the post-ischemic day 4 samples, suggesting the transcription activation in most of the glutamatergic neuron clusters on day 4 after stroke onset (Figure 5C). Comparing the gene expression profiles between sham-operated and day 4 post-ischemic *Padi4*flox/flox mice by using all of the clusters obtained from these mice, we observed that the significantly upregulated genes in glutamatergic neurons on day 4 after stroke onset were enriched with the biological processes associated with nervous system development or synaptic modulation (Figure 5D). We then compared each of the neuronal clusters on the gene expression profiles involved in these gene ontology (GO) terms associated with recovery processes after brain injury, such as nervous tissue reconstruction, synaptic organization, and remyelination (recovery process-associated genes and ontologies are listed in Data file S1). Increased expression levels of the genes annotated by these GO terms, in contrast to other genes, were observed in all of the glutamatergic neuronal clusters of day 4 post-ischemic *Padi4*flox/flox mice compared with sham-operated mice (Figures 5E and S5A). By contrast, neuronal *Padi4* deficiency decreased these gene expression levels in all of the clusters except cluster 5 (Figure 5E), demonstrating that neuronal *Padi4*

deficiency considerably failed to induce the peri-infarct neuronal clusters associated with recovery processes after brain injury.

It is of note that the gene expression profiles associated with these ontology terms were most frequently observed in cluster 4, which was unique in the day 4 post-ischemic brains of *Padi4*flox/flox mice but rarely observed in those of *Vglut1-Cre*; *Vgat-Cre*; *Padi4*flox/flox mice or sham-operated mice (Figures 5E and 5F). We further identified several neuroprotective or neurotrophic factors (*Nr4a2*, *Bdnf*, *Kitl*, and *Gfra1*)[7,11,42,43] as markers for the cluster 4 glutamatergic neurons (Figure 5G). Expression of these marker genes could be detected in PADI4-positive surviving neurons around the peri-infarct region by immunohistochemistry (Figure 5H), indicating the pivotal roles of PADI4 in inducing cluster 4 glutamatergic neurons.

Bulk RNA-seq analysis of peri-infarct neurons revealed the significantly decreased expression of many genes associated with the pro-survival function in neuron and nervous system reconstruction[44–49] in *Vglut1-Cre*; *Vgat-Cre*; *Padi4*flox/flox mice (Figure 5I). By the assay for transposase-accessible chromatin with high-throughput sequencing (ATAC-seq) combined with cleavage under targets and tagmentation (CUT&Tag), an immunotethering assay improved from ChIP-seq, we found that histone-3-citrullinated sites in the day 4 peri-infarct neurons of *Padi4*flox/flox mice were largely different from those in neurons of sham-operated *Padi4*flox/flox or day 4 peri-infarct neurons of *Vglut1-Cre*; *Vgat-Cre*; *Padi4*flox/flox mice (Figure S5B). As shown in Figures 5J and S5C, the histone-citrullinated sites in the day 4 peri-infarct neurons of *Padi4*flox/flox mice were correlated with the

A Glutamatergic neurons

B
- Sham (1709 cells)
- Day 4 *Padi4*^{flox/flox} - 1 (1592 cells)
- Day 4 *Padi4*^{flox/flox} - 2 (601 cells)
- Day 4 *Vglut1-Cre; Vgat-Cre; Padi4*^{flox/flox} - 1 (1346 cells)
- Day 4 *Vglut1-Cre; Vgat-Cre; Padi4*^{flox/flox} - 2 (3066 cells)

C

D

E Gene expression associated with recovery (z-score)

F Sham — Day 4 *Padi4*^{flox/flox} — Day 4 *Vglut1-Cre; Vgat-Cre; Padi4*^{flox/flox}

G *Nr4a2* — *Gfra1* — *Bdnf* — *Kitl*

H Peri-infarct area

I

J Day4 *Padi4*^{flox/flox}

K

(legend on next page)

open chromatin regions of recovery process-associated gene (Data file S1) loci rather than in other gene loci. The intensities of the ATAC-seq signals in gene loci were correlated with their mRNA expression levels detected by RNA-seq in the day 4 peri-infarct neurons of $Padi4^{flox/flox}$ mice (Figure 5K), revealing that histone citrullination by PADI4 had the potential for transcriptional activation of recovery process-associated genes in peri-infarct neurons.

PLA2G2E increases DGLA and its metabolites to induce neuronal PADI4 expression

Next, we attempted to identify the intracerebral fatty acids and their metabolites that induce neuronal PADI4 expression. Mass spectrometry analysis of fatty acids and lysophospholipids obtained from the ischemic brain revealed that only DGLA level was significantly decreased by $Pla2g2e$ deficiency from day 3 to day 6 after stroke onset compared with WT mice (Figure 6A). Among lysophospholipids, the levels of lysophosphatidylserine species (LPS 16:0, LPS 18:1, and LPS 20:1) were significantly decreased by $Pla2g2e$ deficiency on day 3 after stroke onset (Figure 6B), indicating that phosphatidylserine, a dead cell marker specifically exposed on the surface of the cellular membrane in dying cells or cellular debris, was preferably metabolized by secreted PLA2G2E. Therefore, we examined whether DGLA administration could reverse the impaired functional recovery of $Pla2g2e$-deficient mice.

The administration of DGLA recovered the neurological deficits of $Pla2g2e$-deficient mice to a similar level as WT mice; by contrast, the administration of vehicle or stearic acid (as a control lipid) did not improve the neurological deficits of $Pla2g2e$-deficient mice (Figure 6C). PADI4-positive neurons were rarely observed in the peri-infarct area of $Pla2g2e$-deficient mice (Figure 6D), whereas DGLA administration significantly increased the number of PADI4-positive peri-infarct neurons (Figure 6D), resulting in a reduced infarct volume of a similar level to WT mice (Figure 6E; Table S4). DGLA administration did not induce PADI4 expression in the neurons of the normal brain region, indicating that both ischemic stresses and DGLA are necessary for PADI4 expression in peri-infarct neurons.

To compare the $Padi4$-inducing activity of DGLA and its metabolites with various fatty acid metabolites, we measured the luciferase-transcription activity under the $Padi4$ gene promoter using a neuronal cell line. We found that DGLA and its metabolites more commonly had $Padi4$-inducing activity compared with others (Figures 6F and S6). Focusing on DGLA metabolites, we discovered that 15-HETrE had the strongest $Padi4$-inducing activity (Figure 6G). In a mouse model of ischemic stroke, the amount of 15-HETrE in brain tissue increased after stroke onset, and this increase was marked on day 6 (Figure 6H). Mass spectrometry imaging revealed that 15-HETrE was detected in the infarct region on day 3 after stroke onset but was more marked in the surviving brain tissue around the infarct region, as confirmed by hematoxylin and eosin staining or ATP detection (Figure 6I). We found that $Pla2g2e$ deficiency significantly decreased the amount of 15-HETrE in the ischemic brain tissue compared with WT on day 3 after stroke onset (Figure 6J), despite the slightly increased expression level of 15-lipoxygenase ($Alox8$ in mice) that was considered to catalyze DGLA to 15-HETrE in $Pla2g2e$-deficient brain tissue (Figure 6K). These results suggest the possibility that 15-HETrE generated by PLA2G2E participates in the induction of PADI4 expression in peri-infarct neurons. Therefore, we examined whether the administration of 15-HETrE enhanced functional recovery after ischemic brain injury.

15-HETrE promotes functional recovery after ischemic stroke through neuronal PADI4

We administered 15-HETrE to a mouse model of ischemic stroke 24 h after stroke onset. The long-term neurological deficits examined by the corner test and the cylinder test were significantly improved by 15-HETrE administration (Figure 7A). We also observed a significant reduction of the infarct volume in 15-HETrE-administered mice on day 28 after stroke onset (Figure 7B; Tables S5A and S5B). Next, we investigated the effect of 15-HETrE administration on inducing PADI4-positive peri-infarct neurons on day 4 after stroke onset and promoting the neuronal gene expression associated with recovery processes after ischemic brain injury. 15-HETrE administration significantly increased the number of PADI4-positive surviving neurons in the peri-infarct region (Figure 7C). Notably, the number of NR4A2- or BDNF-positive PADI4+ neurons was also significantly increased by 15-HETrE administration (Figure 7D), indicating that 15-HETrE

Figure 5. PADI4-induced peri-infarct neuronal clusters associated with recovery processes after brain injury

(A and B) (A) UMAP of 8,314 glutamatergic neurons and (B) UMAP of each sample collected from the sham-operated brain or peri-infarct region of day 4 post-ischemic brain.

(C) Comparison of the unspliced/spliced mRNA ratio among each sample. Clusters 4 and 10 could not be obtained from the sham-operated brain.

(D) GO terms enriched in the significantly upregulated genes in day 4 post-ischemic glutamatergic neurons of $Padi4^{flox/flox}$ mice compared with sham-operated $Padi4^{flox/flox}$ mice.

(E) Bubble heatmap chart showing the read ratio of genes that belong to the gene ontologies associated with recovery processes after brain injury. The size of the circles indicates the percentage of neurons that belong to each cluster.

(F and G) (F) UMAP of each representative sample and (G) heatmap showing the representative genes highly expressed in the cluster 4 glutamatergic neurons (indicated by arrowhead).

(H) Immunohistochemistry of PADI4 and genes highly expressed in cluster 4 neurons in the peri-infarct region on day 4 after stroke onset. Scale bars, 10 μm.

(I) Volcano plot showing the relative mRNA expression levels in the neurons collected from day 4 peri-infarct regions between $Padi4^{flox/flox}$ and $Vglut1$-Cre; $Vgat$-Cre; $Padi4^{flox/flox}$ mice (n = 3 for each group).

(J) Comparison of averaged ATAC-seq signal intensity around the histone-citrullinated site between the recovery process-associated gene (reparative gene) loci and other gene loci in the peri-infarct neurons of $Padi4^{flox/flox}$ mice on day 4 after stroke onset.

(K) Correlation between ATAC-seq signal intensity (area under the curve [AUC]) and mRNA expression levels detected by RNA-seq in the neurons collected from day 4 peri-infarct regions of $Padi4^{flox/flox}$ mice. Each circle indicates the value of each gene whose ATAC-seq signal peak was detected by the peak-calling.
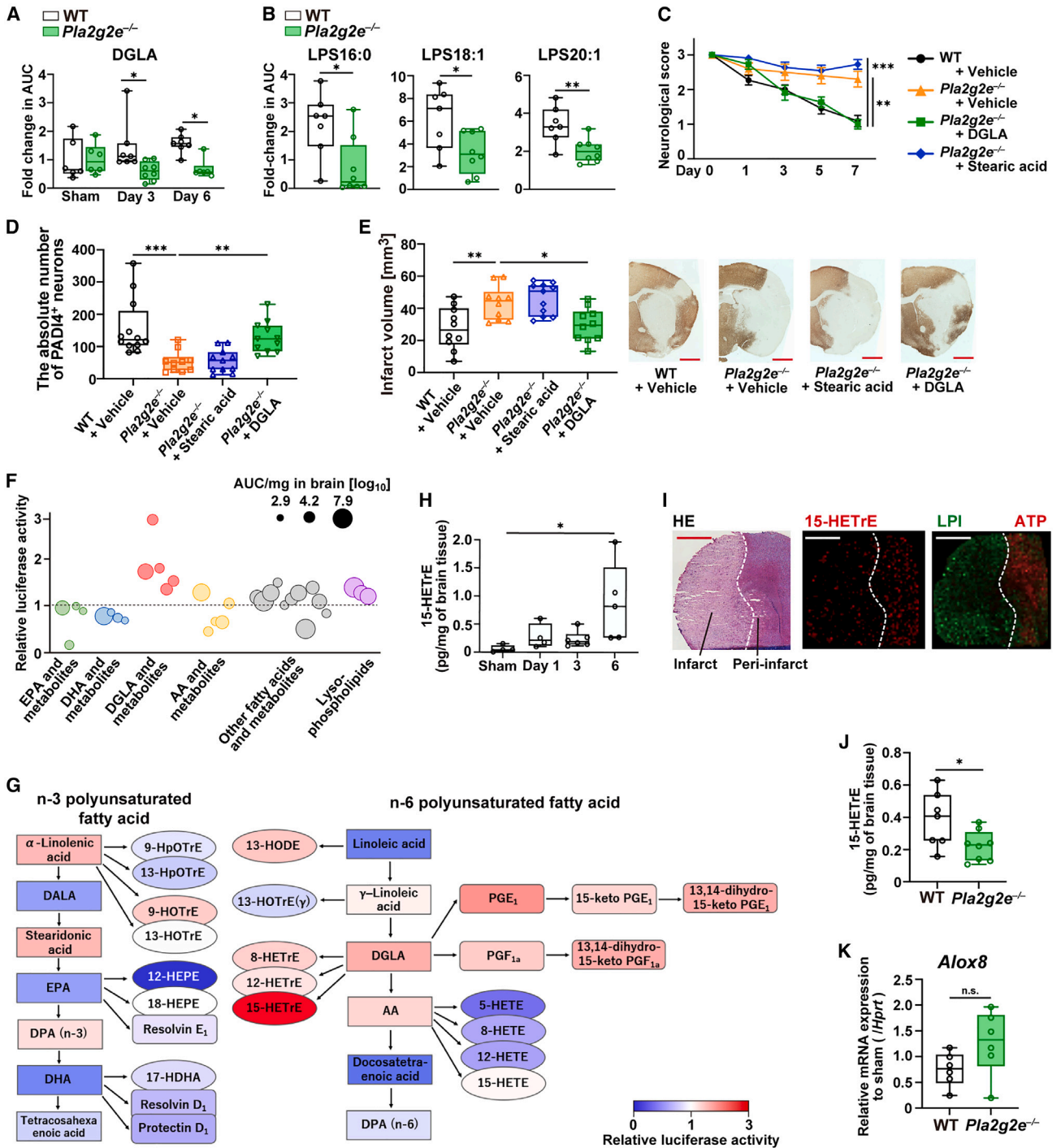
Figure 6. PLA2G2E generated DGLA and its metabolites to promote neuronal PADI4

(A) Time-dependent changes of DGLA in the brain tissue before and after ischemic stroke between WT and *Pla2g2e*-deficient mice. Values are relative to sham-operated WT mice.

(B) The comparison of lysophosphatidylserine species in day 3 post-ischemic brain tissue.

(C–E) (C) Neurological scores after stroke onset, (D) absolute number of Padi4-positive neurons in the peri-infarct region on day 4, and (E) infarct volume on day 4 in each type of mice (n = 12 for vehicle-administered WT, 10 for vehicle-administered *Pla2g2e*$^{-/-}$, 11 for DGLA-administered *Pla2g2e*$^{-/-}$, 11 for stearic-acid-administered *Pla2g2e*$^{-/-}$ mice). Scale bars, 1 mm.

(F) Bubble plots showing the luciferase reporter activities under the *Padi4* gene promoter in Neuro2a cells. The size of the circles indicates the relative levels of fatty acid metabolites in day 3 post-ischemic brain tissue.

(legend continued on next page)

promoted the formation of the peri-infarct neuronal population necessary for recovery processes (as shown in Figure 5H). Consistent with this, the RNA-seq analysis of the neurons collected from the day 4 peri-infarct region revealed apparent enrichment in gene expression associated with nervous system reconstruction and synaptic organization in 15-HETrE-administered mice (Figure 7E).

A significant reduction in the infarct volume and improvement in neurological deficits were observed even on day 4 after stroke onset in 15-HETrE-administered WT mice (Figures 7F and 7G; Table S5C). These therapeutic effects of 15-HETrE administration were confirmed in aged mice, female mice, and photothrombotic stroke model mice without affecting physiological status (Figure S7). However, therapeutic effects were not observed in *Vglut1-Cre*; *Vgat-Cre*; *Padi4*flox/flox mice (Figures 7H and 7I; Tables S5D and S5E), demonstrating that 15-HETrE had pro-survival and pro-reparative effects in peri-infarct neuron against ischemic brain injury through neuronal PADI4. We examined the effects of lipid-signaling inhibitors or agonists on *Padi4* expression in ischemic brain tissue and found that PPARγ was important for PADI4 expression in peri-infarct neurons (Figures S8A and S8B). The number of PADI4-positive peri-infarct neurons was significantly decreased by neuron-specific *Pparg*-deficiency (Figures S8C and S8D). 15-HETrE administration did not improve the infarct volume or neurological deficits in *Vglut1-Cre*; *Vgat-Cre*; *Pparg*flox/flox mice (Figures 7J and 7K; Tables S5F and S5G), demonstrating that 15-HETrE exerted therapeutic effects through PPARγ.

DISCUSSION

The neurons around an injured region have been expected to play major roles in promoting functional recovery through nervous system development, synapse organization, remyelination, and so on[3,4,8–11,16]; however, the potential brain-autonomous molecular mechanisms triggering such a broad range of neural repair after brain injury remained to be clarified. In this study, we first demonstrated that the secretion of PLA2G2E from perilesional neurons generates DGLA and 15-HETrE, which triggers these neural repairs through the neuronal PADI4-dependent induction of neuronal cluster formation associated with recovery processes after ischemic brain injury.

PLA2G2E has been reported to preferentially hydrolyze phosphatidylserine or phosphatidylethanolamine[27]; therefore, it is reasonable that PLA2G2E produced after ischemic stroke preferentially metabolizes the phosphatidylserine markedly exposed on the surface of dead cells in necrotic brain tissue. Although PLA2G4A (group IVA cPLA2α) exaggerates ischemic brain injury by generating AA-derived pro-inflammatory eicosanoids, the cerebral function of PLA2G4E (group IVE cPLA2ε) generating N-acylethanolamine or PLA2G5 (group V sPLA2) expressed in anti-inflammatory macrophages has not been clarified.[22,26–28] Thus, our study clarifies the previously unknown function of PLA2G2E, which generates DGLA and 15-HETrE, triggering brain-autonomous neural repair after ischemic brain injury. We also discovered that PLA2G2E expression was induced through MYD88 and TRIF signaling pathways in the ischemic brain. Both MYD88 and TRIF are core components of the signaling pathways, which are essential for activating immune cells to trigger cerebral post-ischemic inflammation.[33] However, a previous paper reported that the deficiency of *Myd88* or *Trif* genes did not reduce infarct volume,[34] indicating that the MYD88 and TRIF signaling pathway were also important for neuroprotection, whereas its mechanisms remain to be clarified. We also performed bone marrow chimera experiments using *Myd88*/*Trif*-deficient mice and found that MYD88 and TRIF signaling pathways in both hematopoietic cells and brain cells are necessary for *Pla2g2e* mRNA expression in ischemic brain tissue (data not shown). Thus, our study clarified that MYD88 and TRIF signaling pathways in the ischemic brain integrally induce the *Pla2g2e* expression in peri-infarct neurons to prevent additional neuronal damage and excess inflammation.

PADI4 expression was primarily observed in cortical neurons, even when infarcts were mostly localized in the subcortical regions, suggesting ischemia-induced neural repair mechanisms for the compensation of lost brain function. PADI4 is a global transcription regulator in various biological situations.[36–39] PADI4 citrullinated the amine residues of substrate proteins to lose the positive charge, altering protein conformations and interactions with molecules.[38,50] PADI4 activity is known to have a great influence on transcription since the PADI4-dependent citrullination of histone proteins dynamically regulates the open-chromatin or heterochromatin state of various gene loci.[36,37] Although the enzymatic activity of PADI4 is calcium-dependent,[50] ischemic stress may increase intracellular calcium in neurons, which is favorable for PADI4 activity. PADI4-mediated histone citrullination was correlated with the transcriptional activation of recovery process-associated gene loci, rather than other gene loci, in peri-infarct neurons, including neuronal cluster 4 detected by scRNA-seq (Figures 5E and 5F). Marker genes of neural stem/precursor cells were not detected in the genes enriched in neuronal cluster 4, suggesting that the PADI4-dependent transcriptional regulation altered the function of neurons that originally existed around the injured region. It is of note that PADI4 activity in neutrophils or macrophages did not significantly affect ischemic brain damage. A recent study reported that the systemic administration of PADI4 inhibitor is therapeutic against ischemic stroke,[40]

(G) Heatmap showing the *Padi4*-inducing activities of n-3 and n-6 polyunsaturated fatty acids and their metabolites lined up according to the estimated metabolic processes (square: fatty acids, ellipse or rounded square: fatty acid metabolites).

(H) The time-dependent changes of 15-HETrE amount in the brain tissue before and after ischemic stroke.

(I) Mass imaging of 15-HETrE in day 4 post-ischemic brain. Peri-infarct surviving area or infarct region was detected by imaging of ATP or lysophosphatidylinositol (LPI), respectively. Scale bars, 1 mm.

(J and K) (J) 15-HETrE amounts and (K) mRNA expression levels of *Alox8* (15-LOX2) in day 3 post-ischemic brain tissue.

*p < 0.05, **p < 0.01, ***p < 0.001 vs. sham-operated WT brain (A, B, and H), DGLA-administered *Pla2g2e*−/− mice (C), vehicle-administered *Pla2g2e*−/− mice (D and E), Neuro2a with vehicle (G), or WT mice (J and K) (two-way ANOVA with Sidak test, A; two-way ANOVA with Tukey's test, C; Kruskal-Wallis test with Dunn's test, D and H; one-way ANOVA with Dunnett's test, E; or two-sided Student's t test, B, J, and K). Error bars represent the mean ± the standard error of the mean (SEM).
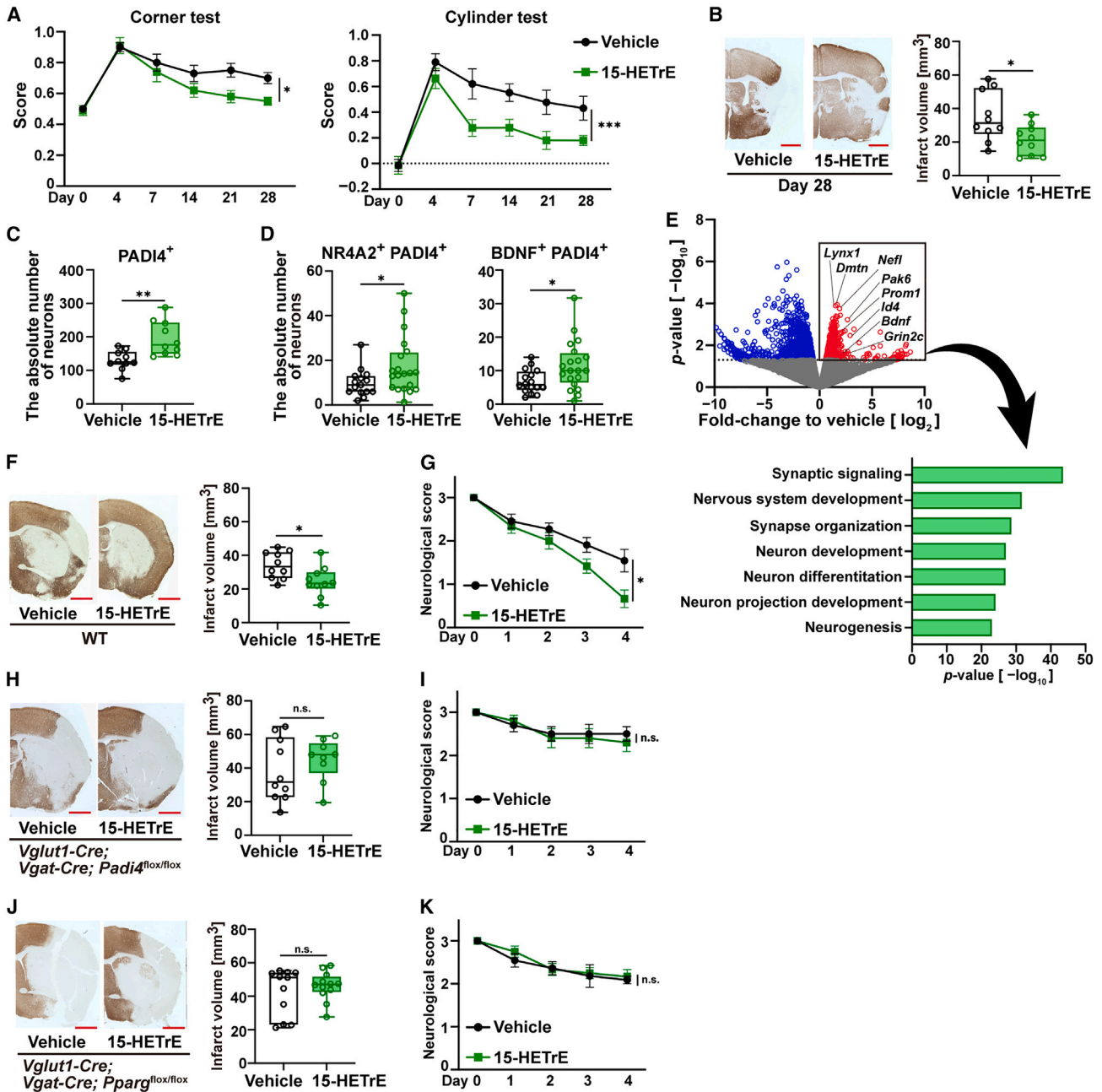
Figure 7. 15-HETrE enhanced functional recovery after ischemic stroke through neuronal PADI4

(A and B) The examination of long-term neurological deficits (A) or infarct volume on day 28 after stroke onset (B) in vehicle- or 15-HETrE-administered mice. (n = 10 for vehicle-administered, 10 for 15-HETrE-administered mice.) Scale bars, 1 mm.

(C and D) (C) The absolute number of PADI4-positive neurons and (D) the absolute number of NR4A2- or BDNF-positive PADI4^{+} neurons in the day 4 peri-infarct region.

(E) Volcano plot showing the relative mRNA expression levels in the neuronal cells collected from day 4 peri-infarct regions between vehicle- and 15-HETrE-administered mice (left). Gene ontologies enriched in the genes whose expressions were significantly increased in 15-HETrE-administered mice (right) (n = 3 for each group).

(F and G) (F) Infarct volume on day 4 and (G) neurological deficits after stroke onset in vehicle- or 15-HETrE-administered WT mice (n = 10 for vehicle-administered, 10 for 15-HETrE-administered mice). Scale bars, 1 mm.

(H and I) (H) Infarct volume on day 4 and (I) neurological deficits after stroke onset in vehicle- or 15-HETrE-administered *Vglut1-Cre*; *Vgat-Cre*; *Padi4*[flox/flox] mice. (n = 10 for vehicle-administered, 9 for 15-HETrE-administered *Vglut1-Cre*; *Vgat-Cre*; *Padi4*[flox/flox] mice.) Scale bars, 1 mm.

(legend continued on next page)

suggesting that the peripheral inhibition of PADI4 activity may be therapeutic since the intravascular formation of neutrophil extracellular traps promotes the coagulation that decreases collateral blood flow around the ischemic lesion.[51]

Few functions of DGLA or 15-HETrE in the brain have been identified to date, although it has been reported that a low serum level of DGLA is related to patients with cardioembolic stroke or mild cognitive impairment.[31,52] Diabetes mellitus, aging, and familial genetic variants are considered to be potential risk factors for DGLA deficiency.[53] DGLA is accumulated in brain tissue by oral intake without conversion into AA,[29] suggesting the potential of dietary therapy using DGLA or 15-HETrE to prevent severe neurological impairment in stroke and neurocognitive disorder, two major causes of reduced healthy life expectancy. Although detailed clinical studies are needed, our findings may change the current paradigm, which holds that only EPA or DHA is beneficial for preventing atherosclerosis and vascular diseases.

STAR★METHODS

Detailed methods are provided in the online version of this paper and include the following:

- KEY RESOURCES TABLE
- RESOURCE AVAILABILITY
  - Lead contact
  - Materials availability
  - Data and code availability
- EXPERIMENTAL MODEL AND SUBJECT DETAILS
  - Mice
  - Mouse model of ischemic stroke
  - Assessments of neuronal injury
- METHOD DETAILS
  - Lipidomics analysis
  - Microarray
  - Quantitative polymerase chain reaction (qPCR)
  - Isolation of the immune cell-enriched population
  - Isolation of neuronal cells from the adult brain
  - RNA-seq
  - scRNA-seq
  - ATAC-seq
  - CUT&Tag (Cleavage under targets and tagmentation)
  - Padi4 luciferase reporter assay
  - Lipid administration
  - Immunohistochemistry
  - MS imaging
- QUANTIFICATION AND STATISTICAL ANALYSIS

SUPPLEMENTAL INFORMATION

Supplemental information can be found online at https://doi.org/10.1016/j.neuron.2023.06.024.

REFERENCES

1. Powers, W.J. (2020). Acute ischemic stroke. N. Engl. J. Med. *383*, 252–260. https://doi.org/10.1056/NEJMcp1917030.

2. Iadecola, C., Buckwalter, M.S., and Anrather, J. (2020). Immune responses to stroke: mechanisms, modulation, and therapeutic potential. J. Clin. Invest. *130*, 2777–2788. https://doi.org/10.1172/JCI135530.

3. Moskowitz, M.A., Lo, E.H., and Iadecola, C. (2010). The science of stroke: mechanisms in search of treatments. Neuron *67*, 181–198. https://doi.org/10.1016/j.neuron.2010.07.002.

4. Langhorne, P., Bernhardt, J., and Kwakkel, G. (2011). Stroke rehabilitation. Lancet *377*, 1693–1702. https://doi.org/10.1016/S0140-6736(11)60325-5.

5. Jin, Y., Dougherty, S.E., Wood, K., Sun, L., Cudmore, R.H., Abdalla, A., Kannan, G., Pletnikov, M., Hashemi, P., and Linden, D.J. (2016). Regrowth of serotonin axons in the adult mouse brain following injury. Neuron *91*, 748–762. https://doi.org/10.1016/j.neuron.2016.07.024.

(J and K) (J) Infarct volume on day 4 and (K) neurological deficits after stroke onset in vehicle- or 15-HETrE-administered *Vglut1-Cre*; *Vgat-Cre*; *Pparg*^flox/flox mice (n = 11 for vehicle-administered, 12 for 15-HETrE-administered *Vglut1-Cre*; *Vgat-Cre*; *Pparg*^flox/flox mice). Scale bars, 1 mm.

*p < 0.05, **p < 0.01, ***p < 0.001 vs. vehicle-administered WT mice (A–D, F, and G), vehicle-administered *Vglut1-Cre*; *Vgat-Cre*; *Padi4*^flox/flox mice (H and I), or vehicle-administered *Vglut1-Cre*; *Vgat-Cre*; *Pparg*^flox/flox mice (J and K) (two-way ANOVA, A, G, I, and K; two-sided Student's t test [B, C, F, and H, BDNF⁺ PADI4⁺ neurons of D]; Mann-Whitney U test [J, NR4A2⁺ PADI4⁺ neurons of D]). n.s., not significant. Error bars represent the mean ± the standard error of the mean (SEM).

6. Canter, R.G., Penney, J., and Tsai, L.-H. (2016). The road to restoring neural circuits for the treatment of Alzheimer's disease. Nature 539, 187–196. https://doi.org/10.1038/nature20412.

7. Sakai, S., and Shichita, T. (2019). Inflammation and neural repair after ischemic brain injury. Neurochem. Int. 130, 104316. https://doi.org/10.1016/j.neuint.2018.10.013.

8. Joy, M.T., Ben Assayag, E.B., Shabashov-Stone, D., Liraz-Zaltsman, S., Mazzitelli, J., Arenas, M., Abduljawad, N., Kliper, E., Korczyn, A.D., Thareja, N.S., et al. (2019). CCR5 is a therapeutic target for recovery after stroke and traumatic brain injury. Cell 176, 1143–1157.e13. https://doi.org/10.1016/j.cell.2019.01.044.

9. Abe, H., Jitsuki, S., Nakajima, W., Murata, Y., Jitsuki-Takahashi, A., Katsuno, Y., Tada, H., Sano, A., Suyama, K., Mochizuki, N., et al. (2018). CRMP2-binding compound, edonerpic maleate, accelerates motor function recovery from brain damage. Science 360, 50–57. https://doi.org/10.1126/science.aao2300.

10. Joy, M.T., and Carmichael, S.T. (2021). Encouraging an excitable brain state: mechanisms of brain repair in stroke. Nat. Rev. Neurosci. 22, 38–53. https://doi.org/10.1038/s41583-020-00396-7.

11. Takase, H., and Regenhardt, R.W. (2021). Motor tract reorganization after acute central nervous system injury: a translational perspective. Neural Regen. Res. 16, 1144–1149. https://doi.org/10.4103/1673-5374.300330.

12. Ortiz, F.C., Habermacher, C., Graciarena, M., Houry, P.-Y., Nishiyama, A., Nait Oumesmar, B., and Angulo, M.C. (2019). Neuronal activity in vivo enhances functional myelin repair. JCI Insight 5, e123434. https://doi.org/10.1172/jci.insight.123434.

13. Poplawski, G.H.D., Kawaguchi, R., Van Niekerk, E.V., Lu, P., Mehta, N., Canete, P., Lie, R., Dragatsis, I., Meves, J.M., Zheng, B., et al. (2020). Injured adult neurons regress to an embryonic transcriptional growth state. Nature 581, 77–82. https://doi.org/10.1038/s41586-020-2200-5.

14. Silasi, G., and Murphy, T.H. (2014). Stroke and the connectome: how connectivity guides therapeutic intervention. Neuron 83, 1354–1368. https://doi.org/10.1016/j.neuron.2014.08.052.

15. Mahar, M., and Cavalli, V. (2018). Intrinsic mechanisms of neuronal axon regeneration. Nat. Rev. Neurosci. 19, 323–337. https://doi.org/10.1038/s41583-018-0001-8.

16. Wahl, A.S., Omlor, W., Rubio, J.C., Chen, J.L., Zheng, H., Schröter, A., Gullo, M., Weinmann, O., Kobayashi, K., Helmchen, F., et al. (2014). Neuronal repair. Asynchronous therapy restores motor control by rewiring of the rat corticospinal tract after stroke. Science 344, 1250–1255. https://doi.org/10.1126/science.1253050.

17. Chen, G.Y., and Nuñez, G. (2010). Sterile inflammation: sensing and reacting to damage. Nat. Rev. Immunol. 10, 826–837. https://doi.org/10.1038/nri2873.

18. Kono, H., and Rock, K.L. (2008). How dying cells alert the immune system to danger. Nat. Rev. Immunol. 8, 279–289. https://doi.org/10.1038/nri2215.

19. Nakamura, K., Sakai, S., Tsuyama, J., Nakamura, A., Otani, K., Kurabayashi, K., Yogiashi, Y., Masai, H., and Shichita, T. (2021). Extracellular DJ-1 induces sterile inflammation in the ischemic brain. PLoS Biol. 19, e3000939. https://doi.org/10.1371/journal.pbio.3000939.

20. Shichita, T., Hasegawa, E., Kimura, A., Morita, R., Sakaguchi, R., Takada, I., Sekiya, T., Ooboshi, H., Kitazono, T., Yanagawa, T., et al. (2012). Peroxiredoxin family proteins are key initiators of post-ischemic inflammation in the brain. Nat. Med. 18, 911–917. https://doi.org/10.1038/nm.2749.

21. Shichita, T., Ito, M., Morita, R., Komai, K., Noguchi, Y., Ooboshi, H., Koshida, R., Takahashi, S., Kodama, T., and Yoshimura, A. (2017). MAFB prevents excess inflammation after ischemic stroke by accelerating clearance of damage signals through MSR1. Nat. Med. 23, 723–732. https://doi.org/10.1038/nm.4312.

22. Bonventre, J.V., Huang, Z., Taheri, M.R., O'Leary, E., Li, E., Moskowitz, M.A., and Sapirstein, A. (1997). Reduced fertility and postischaemic brain injury in mice deficient in cytosolic phospholipase A2. Nature 390, 622–625. https://doi.org/10.1038/37635.

23. Buckley, C.D., Gilroy, D.W., Serhan, C.N., Stockinger, B., and Tak, P.P. (2013). The resolution of inflammation. Nat. Rev. Immunol. 13, 59–66. https://doi.org/10.1038/nri3362.

24. Dalli, J., Chiang, N., and Serhan, C.N. (2015). Elucidation of novel 13-series resolvins that increase with atorvastatin and clear infections. Nat. Med. 21, 1071–1075. https://doi.org/10.1038/nm.3911.

25. Serhan, C.N. (2014). Pro-resolving lipid mediators are leads for resolution physiology. Nature 510, 92–101. https://doi.org/10.1038/nature13479.

26. Murakami, M., Taketomi, Y., Miki, Y., Sato, H., Hirabayashi, T., and Yamamoto, K. (2011). Recent progress in phospholipase A$_2$ research: from cells to animals to humans. Prog. Lipid Res. 50, 152–192. https://doi.org/10.1016/j.plipres.2010.12.001.

27. Sato, H., Taketomi, Y., Ushida, A., Isogai, Y., Kojima, T., Hirabayashi, T., Miki, Y., Yamamoto, K., Nishito, Y., Kobayashi, T., et al. (2014). The adipocyte-inducible secreted phospholipases PLA2G5 and PLA2G2E play distinct roles in obesity. Cell Metab. 20, 119–132. https://doi.org/10.1016/j.cmet.2014.05.002.

28. Murase, R., Sato, H., Yamamoto, K., Ushida, A., Nishito, Y., Ikeda, K., Kobayashi, T., Yamamoto, T., Taketomi, Y., and Murakami, M. (2016). Group X secreted phospholipase A2 releases ω3 polyunsaturated fatty acids, suppresses colitis, and promotes sperm fertility. J. Biol. Chem. 291, 6895–6911. https://doi.org/10.1074/jbc.M116.715672.

29. Umeda-Sawada, R., Fujiwara, Y., Ushiyama, I., Sagawa, S., Morimitsu, Y., Kawashima, H., Ono, Y., Kiso, Y., Matsumoto, A., and Seyama, Y. (2006). Distribution and metabolism of dihomo-γ-linolenic Acid (DGLA, 20:3n-6) by oral supplementation in rats. Biosci. Biotechnol. Biochem. 70, 2121–2130. https://doi.org/10.1271/bbb.60057.

30. Joffre, C., Grégoire, S., Smedt, V.D., Acar, N., Bretillon, L., Nadjar, A., and Layé, S. (2016). Modulation of brain PUFA content in different experimental models of mice. Prostaglandins Leukot. Essent. Fat Acids 114, 1–10. https://doi.org/10.1016/j.plefa.2016.09.003.

31. Mishina, M., Kim, K., Kominami, S., Mizunari, T., Kobayashi, S., and Katayama, Y. (2013). Impact of polyunsaturated fatty acid consumption prior to ischemic stroke. Acta Neurol. Scand. 127, 181–185. https://doi.org/10.1111/j.1600-0404.2012.01695.x.

32. Nicolaou, A., Northoff, B.H., Sass, K., Ernst, J., Kohlmaier, A., Krohn, K., Wolfrum, C., Teupser, D., and Holdt, L.M. (2017). Quantitative trait locus mapping in mice identifies phospholipase Pla2g12a as novel atherosclerosis modifier. Atherosclerosis 265, 197–206. https://doi.org/10.1016/j.atherosclerosis.2017.08.030.

33. Singh, V., Roth, S., Veltkamp, R., and Liesz, A. (2016). HMGB1 as a key mediator of immune mechanisms in ischemic stroke. Antioxid. Redox Signal. 24, 635–651. https://doi.org/10.1089/ars.2015.6397.

34. Famakin, B.M., Mou, Y., Ruetzler, C.A., Bembry, J., Maric, D., and Hallenbeck, J.M. (2011). Disruption of downstream MyD88 or TRIF toll-like receptor signaling does not protect against cerebral ischemia. Brain Res. 1388, 148–156. https://doi.org/10.1016/j.brainres.2011.02.074.

35. der Emde, K.B., Dees, W.L., Hiney, J.K., Hill, D.F., Dissen, G.A., Costa, M.E., Moholt-Siebert, M., Ojeda, S.R., Siebert, M.M., and Ojeda, S. (1995). Neurotrophins and the neuroendocrine brain: different neurotrophins sustain anatomically and functionally segregated subsets of hypothalamic dopaminergic neurons. J. Neurosci. 15, 4223–4237. https://doi.org/10.1523/JNEUROSCI.15-06-04223.1995.

36. Christophorou, M.A., Castelo-Branco, G., Halley-Stott, R.P., Oliveira, C.S., Loos, R., Radzisheuskaya, A., Mowen, K.A., Bertone, P., Silva, J.C.R., Zernicka-Goetz, M., et al. (2014). Citrullination regulates pluripotency and histone H1 binding to chromatin. Nature 507, 104–108. https://doi.org/10.1038/nature12942.

37. Kolodziej, S., Kuvardina, O.N., Oellerich, T., Herglotz, J., Backert, I., Kohrs, N., Buscató, E. la, Wittmann, S.K., Salinas-Riester, G., Bonig, H., et al. (2014). PADI4 acts as a coactivator of Tal1 by counteracting

repressive histone arginine methylation. Nat. Commun. 5, 3995. https://doi.org/10.1038/ncomms4995.

38. Slade, D.J., Horibata, S., Coonrod, S.A., and Thompson, P.R. (2014). A novel role for protein arginine deiminase 4 in pluripotency: the emerging role of citrullinated histone H1 in cellular programming. BioEssays 36, 736–740. https://doi.org/10.1002/bies.201400057.

39. Stadler, S.C., Vincent, C.T., Fedorov, V.D., Patsialou, A., Cherrington, B.D., Wakshlag, J.J., Mohanan, S., Zee, B.M., Zhang, X., Garcia, B.A., et al. (2013). Dysregulation of PAD4-mediated citrullination of nuclear GSK3β activates TGF-β signaling and induces epithelial-to-mesenchymal transition in breast cancer cells. Proc. Natl. Acad. Sci. USA 110, 11851–11856. https://doi.org/10.1073/pnas.1308362110.

40. Kim, S.-W., Lee, H., Lee, H.-K., Kim, I.-D., and Lee, J.-K. (2019). Neutrophil extracellular trap induced by HMGB1 exacerbates damages in the ischemic brain. Acta Neuropathol. Commun. 7, 94. https://doi.org/10.1186/s40478-019-0747-x.

41. Tasic, B., Yao, Z., Graybuck, L.T., Smith, K.A., Nguyen, T.N., Bertagnolli, D., Goldy, J., Garren, E., Economo, M.N., Viswanathan, S., et al. (2018). Shared and distinct transcriptomic cell types across neocortical areas. Nature 563, 72–78. https://doi.org/10.1038/s41586-018-0654-5.

42. Kim, S.M., Cho, S.Y., Kim, M.W., Roh, S.R., Shin, H.S., Suh, Y.H., Geum, D., and Lee, M.A. (2020). Genome-wide analysis identifies NURR1-controlled network of new synapse formation and cell cycle arrest in human neural stem cells. Mol. Cells 43, 551–571. https://doi.org/10.14348/molcells.2020.0071.

43. Lipsky, R.H., and Marini, A.M. (2007). Brain-derived neurotrophic factor in neuronal survival and behavior-related plasticity. Ann. N. Y. Acad. Sci. 1122, 130–143. https://doi.org/10.1196/annals.1403.009.

44. Zhang, K., Zhang, Q., Deng, J., Li, J., Li, J., Wen, L., Ma, J., and Li, C. (2019). ALK5 signaling pathway mediates neurogenesis and functional recovery after cerebral ischemia/reperfusion in rats via Gadd45b. Cell Death Dis. 10, 360. https://doi.org/10.1038/s41419-019-1596-z.

45. Chen, C.-H., Lee, A., Liao, C.-P., Liu, Y.-W., and Pan, C.-L. (2014). RHGF-1/PDZ-RhoGEF and retrograde DLK-1 signaling drive neuronal remodeling on microtubule disassembly. Proc. Natl. Acad. Sci. USA 111, 16568–16573. https://doi.org/10.1073/pnas.1410263111.

46. Arac, A., Brownell, S.E., Rothbard, J.B., Chen, C., Ko, R.M., Pereira, M.P., Albers, G.W., Steinman, L., and Steinberg, G.K. (2011). Systemic augmentation of alphaB-crystallin provides therapeutic benefit twelve hours post-stroke onset via immune modulation. Proc. Natl. Acad. Sci. USA 108, 13287–13292. https://doi.org/10.1073/pnas.1107368108.

47. Yang, L., Su, Z., Wang, Z., Li, Z., Shang, Z., Du, H., Liu, G., Qi, D., Yang, Z., Xu, Z., et al. (2021). Transcriptional profiling reveals the transcription factor networks regulating the survival of striatal neurons. Cell Death Dis. 12, 262. https://doi.org/10.1038/s41419-021-03552-8.

48. Lee, Q.Y., Mall, M., Chanda, S., Zhou, B., Sharma, K.S., Schaukowitch, K., Adrian-Segarra, J.M., Grieder, S.D., Kareta, M.S., Wapinski, O.L., et al. (2020). Pro-neuronal activity of Myod1 due to promiscuous binding to neuronal genes. Nat. Cell Biol. 22, 401–411. https://doi.org/10.1038/s41556-020-0490-3.

49. Cheng, Y.C., Snavely, A., Barrett, L.B., Zhang, X., Herman, C., Frost, D.J., Riva, P., Tochitsky, I., Kawaguchi, R., Singh, B., et al. (2021). Topoisomerase I inhibition and peripheral nerve injury induce DNA breaks and ATF3-associated axon regeneration in sensory neurons. Cell Rep. 36, 109666. https://doi.org/10.1016/j.celrep.2021.109666.

50. Arita, K., Hashimoto, H., Shimizu, T., Nakashima, K., Yamada, M., and Sato, M. (2004). Structural basis for Ca2+-induced activation of human PAD4. Nat. Struct. Mol. Biol. 11, 777–783. https://doi.org/10.1038/nsmb799.

51. Gollomp, K., Kim, M., Johnston, I., Hayes, V., Welsh, J., Arepally, G.M., Kahn, M., Lambert, M.P., Cuker, A., Cines, D.B., et al. (2018). Neutrophil accumulation and NET release contribute to thrombosis in HIT. JCI Insight 3, e99445. https://doi.org/10.1172/jci.insight.99445.

52. Ishihara, K., Izawa, K.P., Kitamura, M., Shimogai, T., Kanejima, Y., Morisawa, T., and Shimizu, I. (2020). Serum concentration of dihomo-γ-linolenic acid is associated with cognitive function and mild cognitive impairment in coronary artery disease patients. Prostaglandins Leukot. Essent. Fatty Acids 158, 102038. https://doi.org/10.1016/j.plefa.2019.102038.

53. Hammouda, S., Ghzaiel, I., Khamlaoui, W., Hammami, S., Mhenni, S.Y., Samet, S., Hammami, M., and Zarrouk, A. (2020). Genetic variants in FADS1 and ELOVL2 increase level of arachidonic acid and the risk of Alzheimer's disease in the Tunisian population. Prostaglandins Leukot. Essent. Fatty Acids 160, 102159. https://doi.org/10.1016/j.plefa.2020.102159.

54. Bolger, A.M., Lohse, M., and Usadel, B. (2014). Trimmomatic: a flexible trimmer for Illumina sequence data. Bioinformatics 30, 2114–2120. https://doi.org/10.1093/bioinformatics/btu170.

55. Kim, D., Paggi, J.M., Park, C., Bennett, C., and Salzberg, S.L. (2019). Graph-based genome alignment and genotyping with HISAT2 and HISAT-genotype. Nat Biotechnol 37, 907–915. https://doi.org/10.1038/s41587-019-0201-4.

56. Langmead, B., and Salzberg, S.L. (2012). Fast gapped-read alignment with Bowtie 2. Nat Methods 9, 357–359. https://doi.org/10.1038/nmeth.1923.

57. Liao, Y., Smyth, G.K., and Shi, W. (2014). featureCounts: an efficient general purpose program for assigning sequence reads to genomic features. Bioinformatics 30, 923–930. https://doi.org/10.1093/bioinformatics/btt656.

58. Ramírez, F., Ryan, D.P., Grüning, B., Bhardwaj, V., Kilpert, F., Richter, A.S., Heyne, S., Dündar, F., and Manke, T. (2016). deepTools2: a next generation web server for deep-sequencing data analysis. Nucleic Acids Res, 44. https://doi.org/10.1093/nar/gkw257.

59. Robinson, M.D., McCarthy, D.J., and Smyth, G.K. (2010). edgeR: a Bioconductor package for differential expression analysis of digital gene expression data. Bioinformatics 26, 139–140. https://doi.org/10.1093/bioinformatics/btp616.

60. Satija, R., Farrell, J.A., Gennert, D., Schier, A.F., and Regev, A. (2015). Spatial reconstruction of single-cell gene expression data. Nat Biotechnol 33, 495–502. https://doi.org/10.1038/nbt.3192.

61. La Manno, G., Soldatov, R., Ziesel, A., Braun, E., Hochgerner, H., Petukhov, V., Lidschreiber, K., Kastriti, M.E., Lönnerberg, P., Furlan, A., et al. (2018). RNA velocity of single cells. Nature 560, 494–498. https://doi.org/10.1038/s41586-018-0414-6.

62. He, W., Barak, Y., Hevener, A., Olson, P., Liao, D., Le, J., Nelson, M., Ong, E., Olefsky, J.M., and Evans, R.M. (2003). Adipose-specific peroxisome proliferator-activated receptor γ knockout causes insulin resistance in fat and liver but not in muscle. Proc. Natl. Acad. Sci. USA 100, 15712–15717. https://doi.org/10.1073/pnas.2536828100.

63. Adachi, O., Kawai, T., Takeda, K., Matsumoto, M., Tsutsui, H., Sakagami, M., Nakanishi, K., and Akira, S. (1998). Targeted disruption of the MyD88 gene results in loss of IL-1- and IL-18-mediated function. Immunity 9, 143–150. https://doi.org/10.1016/s1074-7613(00)80596-8.

64. Yamamoto, M., Sato, S., Hemmi, H., Hoshino, K., Kaisho, T., Sanjo, H., Takeuchi, O., Sugiyama, M., Okabe, M., Takeda, K., et al. (2003). Role of adaptor TRIF in the MyD88-independent toll-like receptor signaling pathway. Science 301, 640–643. https://doi.org/10.1126/science.1087262.

65. Scumpia, P.O., Botten, G.A., Norman, J.S., Kelly-Scumpia, K.M., Spreafico, R., Ruccia, A.R., Purbey, P.K., Thomas, B.J., Modlin, R.L., and Smale, S.T. (2017). Opposing roles of toll-like receptor and cytosolic DNA-STING signaling pathways for Staphylococcus aureus cutaneous host defense. PLoS Pathog. 13, e1006496. https://doi.org/10.1371/journal.ppat.1006496.

66. Miki, Y., Yamamoto, K., Taketomi, Y., Sato, H., Shimo, K., Kobayashi, T., Ishikawa, Y., Ishii, T., Nakanishi, H., Ikeda, K., et al. (2013). Lymphoid tissue phospholipase A2 group IID resolves contact hypersensitivity by

driving antiinflammatory lipid mediators. J. Exp. Med. 210, 1217–1234. https://doi.org/10.1084/jem.20121887.

67. Zheng, G.X.Y., Terry, J.M., Belgrader, P., Ryvkin, P., Bent, Z.W., Wilson, R., Ziraldo, S.B., Wheeler, T.D., McDermott, G.P., Zhu, J., et al. (2017). Massively parallel digital transcriptional profiling of single cells. Nat. Commun. 8, 14049. https://doi.org/10.1038/ncomms14049.

68. Hafemeister, C., and Satija, R. (2019). Normalization and variance stabilization of single-cell RNA-seq data using regularized negative binomial regression. Genome Biol. 20, 296. https://doi.org/10.1186/s13059-019-1874-1.

69. Hao, Y., Hao, S., Andersen-Nissen, E., Mauck, W.M., Zheng, S., Butler, A., Lee, M.J., Wilk, A.J., Darby, C., Zager, M., et al. (2021). Integrated analysis of multimodal single-cell data. Cell 184, 3573–3587.e29. https://doi.org/10.1016/j.cell.2021.04.048.

70. Stuart, T., Butler, A., Hoffman, P., Hafemeister, C., Papalexi, E., Mauck, W.M., Hao, Y., Stoeckius, M., Smibert, P., and Satija, R. (2019). Comprehensive integration of single-cell data. Cell 177, 1888–1902.e21. https://doi.org/10.1016/j.cell.2019.05.031.

71. Manno, G.L., Soldatov, R., Zeisel, A., Braun, E., Hochgerner, H., Petukhov, V., Lidschreiber, K., Kastriti, M.E., Lönnerberg, P., Furlan, A., et al. (2018). RNA velocity of single cells. Nature 560, 494–498. https://doi.org/10.1038/s41586-018-0414-6.

72. Buenrostro, J.D., Wu, B., Chang, H.Y., and Greenleaf, W.J. (2015). ATAC-seq: A method for assaying chromatin accessibility genome-wide. Curr. Protoc. Mol. Biol. 109, 21.29.1–21.29.9. https://doi.org/10.1002/0471142727.mb2129s109.

73. Kawashima, H., Tateishi, N., Shiraishi, A., Teraoka, N., Tanaka, T., Tanaka, A., Matsuda, H., and Kiso, Y. (2008). Oral administration of Dihomo-γ-linolenic acid prevents development of atopic dermatitis in NC/Nga mice. Lipids 43, 37–43. https://doi.org/10.1007/s11745-007-3129-2.

STAR★METHODS

KEY RESOURCES TABLE

REAGENT or RESOURCE	SOURCE	IDENTIFIER
Antibodies		
Anti-ACSA2 APC	Miltenyi Biotec	RRID:AB_2727362;Cat#130-116-142
Anti-CD11b PerCP-Cy5.5	eBioscience	RRID:AB_2234066;Cat#M1/70
Anti-CD140a APC	BioLegend	RRID:AB_2043969;Cat#135907
Anti-CD140b APC	BioLegend	RRID:AB_2043971;Cat#136007
Anti-CD31 PE-Cy7	BioLegend	RRID:AB_2572181;Cat#102523
Anti-CD45 FITC	eBioscience	RRID:AB_465050; Cat#11-0451-82
Anti-MARCO RPE	GeneTex	RRID:AB_11164210;Cat#GTX39743
Anti-MSR1 (CD204) APC	Bio-Rad	RRID:AB_2148251;Cat#MCA1322A647T
Anti-O4 APC	Miltenyi Biotec	RRID:AB_2751598;Cat#130-118-978
Anti-Thy1.2 PE	BioLegend	RRID:AB_313178; Cat#105307
Mouse anti-BDNF	Abcam	RRID:AB_2631315;Cat#ab203573
Mouse anti-CaMKII	Abcam	RRID:AB_447192; Cat#ab22609
Mouse anti-GAD67	Millipore	RRID:AB_2278725;Cat#MAB5406
Mouse anti-GFRα-1	Santa Cruz Biotechnology	RRID:AB_10649373;Cat#sc-271546
Mouse anti-NeuN	Millipore	RRID:AB_2298772;Cat#MAB377
Mouse anti-Nurr1	ThermoFisher	RRID:AB_1962646,Cat#N1404
Mouse anti-SCF	Santa Cruz Biotechnology	RRID:AB_628238; Cat#sc-13126
Rabbit anti-PADI4	GeneTex	RRID:AB_2037599;Cat#GTX113945
Rabbit anti-PLA2G2E	Abcam	RRID:N/A; Cat#ab204576
Anti-MAP2	Sigma-Aldrich	RRID:AB_477193; Cat#M4403
Anti-PRX5	Shichita et al.[21]	N/A
Anti-DJ-1	Nakamura et al.[19]	N/A
Anti-PPARγ	Proteintech	RRID:AB_10596794 ; Cat#16643-1-AP
Anti-mouse IgG Alexa Fluor 488	Invitrogen	RRID:AB_2534084;Cat#A11017
Anti-mouse IgG Alexa Fluor 546	Invitrogen	RRID:AB_2534085;Cat#A11018
Anti-rabbit IgG Alexa Fluor 488	Invitrogen	RRID:AB_2534114;Cat#A11070
Anti-rabbit IgG Alexa Fluor 546	Invitrogen	RRID:AB_2534115;Cat#A11071
Rabbit anti-histone H3 (citrulline R2+R8+R17)	Abcam	RRID:AB_304752; Cat#ab5103
Guinea pig anti-rabbit IgG	antibodies-online GmbH	RRID:AB_10775589;Cat#ABIN101961
Biological samples		
Section of human brain tissue, see Table S3	Center for Medical Research Cooperation, Tokyo Metropolitan Institute of Medical Science	N/A
Chemicals, peptides, and recombinant proteins		
Rose Bengal	Sigma-Aldrich	Cat#330000
In Situ Cell Death Detection Kit, TMR red	Sigma-Aldrich	Cat#12156792910
N-Methyl-D(-)-glucamine (NMDG)	Sigma-Aldrich	Cat#M2004
Kynurenic acid	Sigma-Aldrich	Cat#K3375
Lidocaine HCl	Sigma-Aldrich	Cat#L5674
Pronase (protease from *Streptomyces griseus*)	Sigma-Aldrich	Cat#P8811
Collagenase type IV	Sigma-Aldrich	Cat#C5138

(Continued on next page)

Continued

REAGENT or RESOURCE	SOURCE	IDENTIFIER
DNase I	Roche	Cat#10104159001
Percoll	Cytiva	Cat#GE17-0891-01
RNase inhibitor	Nacalai Tesque	Cat#30260-96
Protease inhibitor cocktail	Nacalai Tesque	Cat#25955-11
Proteinase K	Nacalai Tesque	Cat#29442-85
Spermidine	Sigma-Aldrich	Cat#S2501
IGEPALl CA-630	Sigma-Aldrich	Cat#56741
Digitonin	Millipore	Cat300410
pA-Tn5	Prepared as protocol	https://www.protocols.io/view/bench-top-cut-amp-tag-kqdg34qdpl25/v2
SPRIselect	Beckman Coulter	Cat#B3318
Palmitic acid	Sigma-Aldrich	Cat#P9417
Stearic acid	Sigma-Aldrich	Cat#S4651
Palmitoleic acid	Sigma-Aldrich	Cat#P9417
Oleic acid	Sigma-Aldrich	Cat#O1008
5(Z),8(Z),11(Z)-eicosatrienoic acid (mead acid)	Cayman Chemical	Cat#90190
5(S)-HETrE	Cayman Chemical	Cat#36230
A-linolenic acid	Sigma-Aldrich	Cat#L2378
9(S)-HpOTrE	Cayman Chemical	Cat#45120
13(S)-HpOTrE	Cayman Chemical	Cat#45220
9(S)-HOTrE	Cayman Chemical	Cat#39420
13(S)-HOTrE	Cayman Chemical	Cat#39620
11(Z),14(Z),17(Z)-eicosatrienoic acid (DALA)	Cayman Chemical	Cat#90192
Stearidonic acid	Sigma-Aldrich	Cat#SMB00291
Eicosapentaenoic acid (EPA)	Sigma-Aldrich	Cat#E2011
Docosapentaenoic acid (n-3 DPA)	Cayman Chemical	Cat#90165
Docosahexaenoic acid (DHA)	Sigma-Aldrich	Cat#D2534
6(Z),9(Z),12(Z),18(Z),21(Z)-tetracosahexaenoic acid	Cayman Chemical	Cat#10005165
Linoleic acid	Sigma-Aldrich	Cat#L1376
13(S)-HODE	Cayman Chemical	Cat#38610
G-linolenic acid (GLA)	Sigma-Aldrich	Cat#L2378
13(S)-HOTrE (g)	Cayman Chemical	Cat#39610
Prostaglandin E1	Cayman Chemical	Cat#13010
15-keto prostaglandin E1	Cayman Chemical	Cat#13680
13,14-dihydro-15-keto prostaglandin E1	Cayman Chemical	Cat#13650
Dihomo-g-linolenic acid (DGLA)	Cayman Chemical	Cat#90230
8(S)-HETrE	Cayman Chemical	Cat#36360
12(S)-HETrE	Cayman Chemical	Cat#18483
15(S)-HETrE	Cayman Chemical	Cat#36720
Prostaglandin F1a	Cayman Chemical	Cat#15010
13,14-dihydro-15-keto prostaglandin F1a	Cayman Chemical	Cat#15670
Arachidonic acid (AA)	Sigma-Aldrich	Cat#A3611
5(S)-HETE	Cayman Chemical	Cat#34230
8(S)-HETE	Cayman Chemical	Cat#34360
12(S)-HETE	Cayman Chemical	Cat#34570
15(S)-HETE	Cayman Chemical	Cat#34720

Continued

REAGENT or RESOURCE	SOURCE	IDENTIFIER
Docosatetraenoic acid	Sigma-Aldrich	Cat#D3659
All-cis-4,7,10,13,16-docosapentaenoic acid (n6 DPA)	Cayman Chemical	Cat#10008335
16:0 Lyso PC	Avanti	Cat#855675
18:0 Lyso PS	Avanti	Cat#858144
18:0 Lyso PE	Avanti	Cat#856715
Blocking One Histo	Nacalai Tesque	Cat#06349-64
Critical commercial assays		
RNAiso Plus	Takara	Cat#9109
RNeasy Mini Kit	Qiagen	Cat#74104
ReliaPrep RNA Cell Miniprep System	Promega	Cat#Z6010
High-Capacity cDNA Reverse Transcription Kit	Applied Biosystems	Cat#4368814
SsoFast EvaGreen Supermixes	Bio-Rad	Cat#172520
TaqMan Gene Expression Assay	Applied Biosystems	Cat#4331182
Low Input Quick Amp Labeling Kit	Agilent Technologies	Cat#5190-2943
Whole Mouse Genome Microarray Kit 4x44k	Agilent Technologies	Cat#G4122F
Chromium Next GEM Single Cell 3' Reagent Kits v3.1	10x Genomics	Cat#1000120, 1000215, 1000268
Ovation Solo RNA-Seq Library preparation kit	Tecan	Cat#0501
Nextera DNA Library Preparation Kit	Illumina	Cat#FC-121-1030
KAPA HiFi HS ReadyMix	KAPA BIOSYSTEMS	Cat#KK2601
NEBNext High-Fidelity 2X PCR Master Mix	New England BioLabs	Cat#M0541
High Sensitivity DNA kit	Agilent Technologies	Cat#5067-4626
Viofectin Transfection Reagent	Viogene	Cat#VFT1001
Luciferase Assay System	Promega	Cat#E1500
TrueBlack IF Background Suppressor System	Biotium	Cat#23012
Deposited data		
Microarray1 *Pla2g2e*-deficient and wild type mice	This paper	GSE232174
Microarray2 *Pla2g2e*-deficient and wild type mice	This paper	GSE230996
Bulk RNA-seq1 *Padi4*-deficient and wild type mice	This paper	GSE231718
Bulk RNA-seq2 15-HETrE administration	This paper	GSE231400
ATAC-seq data	This paper	GSE232169
CUT&Tag data	This paper	GSE232171
scRNA-seq data	This paper	GSE232429
Mouse reference genome mm10	University of California, Santa Cruz	https://hgdownload.soe.ucsc.edu/downloads.html
Mouse reference genome mm10 for Cell Ranger	10x Genomics	https://support.10xgenomics.com/single-cell-gene-expression/software/release-notes/build#mm10_2020A
Experimental models: Cell lines		
Neuro-2a	JCRB Cell Bank	RRID:CVCL_0470; Cat#IFO50081
Experimental models: Organisms/strains		
B6.Cg-Padi4[tm1.2Kmow]/J (Padi4[flox/flox]) mouse	Jackson Labs	RRID:IMSR_JAX:026708
B6.129P2-Lyz2[tm1(cre)Ifo]/J (LysM-Cre) mouse	Jackson Labs	RRID:IMSR_JAX:004781
B6.129-Pparg[tm2Rev]/J (Pparg[flox/flox]) mouse	Jackson Labs	RRID:IMSR_JAX:004584

(Continued on next page)

Continued

REAGENT or RESOURCE	SOURCE	IDENTIFIER
B6;129S6-Gt(ROSA)26Sor[tm14(CAG-tdTomato)Hze]/J (Ai14) mouse	Jackson Labs	RRID:IMSR_JAX:007908
B6;129S-Slc17a7[tm1.1(cre)Hze]/J (Vglut1-Cre) mouse	Jackson Labs	RRID:IMSR_JAX:023527
B6J.129S6(FVB)-Slc32a1[tm2(cre)Lowl]/MwarJ (Vgat-Cre) mouse	Jackson Labs	RRID:IMSR_JAX:028862
C57BL/6JmsSlc mouse	SLC Japan	N/A
C57BL/6NCrSlc mouse	SLC Japan	N/A
Myd88/Trif double knockout mouse	Oriental BioService	RRID:IMSR_OBS:17
Pla2g2e knockout mouse	Sato et al.[27]	N/A
Pla2g4e knockout mouse	Murase et al.[28]	N/A
Pla2g5 knockout mouse	Sato et al.[27]	N/A
Pla2g10 knockout mouse	Murase et al.[28]	N/A
Pla2g12a knockout mouse	This paper	N/A
Oligonucleotides		
Padi4 promoter cloning forward primer: 5'-AAAACGCGTAACAATGAGTGACCC TGCTTTAACAATGGGGGAGC-3'	This paper	N/A
Padi4 promoter cloning reverse primer: 5'-TTTTGTCGACGCCAGGCGAGCCC ATGAGTCAGCACCT-3'	This paper	N/A
qPCR primers (see the Table S7)	This paper	N/A
Recombinant DNA		
pGL3-Basic plasmid	Promega	Cat#E1751
pGL3-Basic-Padi4-promoter-luciferase plasmid	This paper	N/A
CMV-β-galactosidase plasmid	Shichita et al.[21]	N/A
Software and algorithms		
ImageJ 1.49v	National Institutes of Health	https://imagej.nih.gov/ij/index.html
Trimmomatic 0.39	Bolger et al.[54]	https://github.com/usadellab/Trimmomatic
HISAT2 2.2.1	Kim et al.[55]	http://daehwankimlab.github.io/hisat2/
Bowtie2 2.5.0	Langmead et al.[56]	https://bowtie-bio.sourceforge.net/bowtie2/index.shtml
Subread 2.0.3 (featureCounts)	Liao et al.[57]	https://subread.sourceforge.net/
deepTools 3.5.0 (bamCoverage)	Ramírez et al.[58]	https://deeptools.readthedocs.io/en/develop/#
Genrich 0.6.2	Gaspar. (unpublished)	https://github.com/jsh58/Genrich
Cell Ranger 6.0.1	10x Genomics	https://www.10xgenomics.com/
Loupe Browser 6.0.0	10x Genomics	https://www.10xgenomics.com/
R 4.2.2	R Development Core Team	https://www.r-project.org/
edgeR 3.17	Robinson et al.[59]	https://bioconductor.org/packages/release/bioc/html/edgeR.html
Seurat 4.0.4	Satija et al.[60]	https://satijalab.org/seurat/
Velocyte 0.17.17	La Manno et al.[61]	http://velocyto.org/
Graphpad Prism version 9.5.1 (528)	GraphPad Software	https://www.graphpad.com/
MATLAB 2022	MathWorks	https://mathworks.com/
Other		
DNBSEQG-400,10x library sequence	Azenta Japan	N/A
HiSeq 2500, PE150 sequence	Azenta Japan	N/A

RESOURCE AVAILABILITY

Lead contact

Further information and requests should be directed to and will be fulfilled by the lead contact, Takashi Shichita (shichita-tk@cmn.tmd.ac.jp).

Materials availability

Reagents generated in this study are available from the lead contact upon request.

Data and code availability

Microarray and next generation sequence data are available from Gene Expression Omnibus (GEO) repository. The accession numbers are listed in the key resources table. Any additional information reported in this study is available from the lead contact upon request.

EXPERIMENTAL MODEL AND SUBJECT DETAILS

Mice

Pla2g2e$^{-/-}$, Pla2g4e$^{-/-}$, Pla2g5$^{-/-}$, Pla2g10$^{-/-}$, Pla2g12a$^{-/-}$, *Padi4*$^{flox/flox}$ and *Pparg*$^{flox/flox}$ mice were maintained in a conventional facility at the Tokyo Metropolitan Institute of Medical Science in Tokyo, Japan. All experiments were approved by the Institutional Animal Research Committee of the Tokyo Metropolitan Institute of Medical Science (approval number: 21-004). In the experiments using Pla2g2e$^{-/-}$, Pla2g4e$^{-/-}$, Pla2g5$^{-/-}$, Pla2g10$^{-/-}$, and Pla2g12a$^{-/-}$ mice (C57BL/6N background as described previously[27,28]) or the lipid-administration experiments, wild-type C57BL/6N mice were used as WT for comparison. These mice were kindly provided by Dr. Makoto Murakami and were fed and bred from pups under identical breeding conditions at the Tokyo Metropolitan Institute of Medical Science. *Padi4*$^{flox/flox}$ mice (JAX Stock No: 026708) or Rosa26-CAG-LSL-tdTomato (Ai14, JAX Stock No: 007908) were bred with *LysM-Cre* mice (JAX Stock No: 004781) or *Slc17a7-IRES2-Cre* (*Vglut1-Cre*, JAX Stock No: 023527); *Slc32a1-IRES-Cre* (*Vgat-Cre*, JAX Stock No: 028862) mice several times before using for experiments. *Pparg*$^{flox/flox}$ mice[62] (JAX Stock No: 004584) were bred with *Slc17a7-IRES2-Cre* and *Slc32a1-IRES-Cre* mice (these mice were on C57BL/6J background) several times and used for experiments. Myd88$^{-/-}$/Trif$^{-/-}$ mice on a C57BL/6J background developed by Dr. Shizuo Akira (Osaka University, Japan) were provided by Oriental BioService, Inc.[63–65] In the experiment using Myd88$^{-/-}$/Trif$^{-/-}$ mice, wild-type C57BL/6J mice were used as WT for comparison.

Mouse model of ischemic stroke

Male mice aged 8 to 24 weeks and weighing 20 to 30 g, were randomly selected for experiments except for the experiments of aged mice (aged 19 to 24 months) or female mice. Eight to fifteen mice were estimated to be necessary to reach sufficient statistical power. To generate transient brain ischemia (middle cerebral artery occlusion: MCAO), mice were anesthetized with isoflurane in a mixture of 70% nitrous oxide and 30% oxygen, and then silicon-coated monofilaments were inserted from the common carotid artery. The head temperature was kept at 36°C during the MCAO procedure. Mice in which a greater than 60% reduction in cerebral blood flow was confirmed by laser Doppler flowmetry were included in this study. The number of excluded mice, physiological data, the changes in CBF during ischemia, and the survival rate after MCAO are shown in Supplementary Tables. To allow reperfusion, inserted monofilaments were withdrawn 60 min after MCAO. To generate permanent ischemia (photothrombotic ischemia model), mice were anesthetized with isoflurane in a mixture of 70% nitrous oxide and 30% oxygen. After the head temperature was kept at 36°C, Rose Bengal (Sigma-Aldrich) was intravenously injected at a dose of 20 mg kg^{-1} body weight, and was activated by the focal illumination (2 mm lateral and 1 mm posterior to bregma in right hemisphere) with a green laser (561 nm, 4 mW, Coherent Inc.) for 4 min. After the scalp was sutured, the mice were recovered from anesthesia.

Assessments of neuronal injury

We evaluated the neurological deficits during the early post-ischemic periods in a blinded fashion using the previously described four-point scale method (0 = no observable deficit, 1 = forelimb flexion, 2 = decreased resistance to lateral push without circling, and 3 = same behavior as grade 2, with circling).[19–21] For the assessment of long-term neurological deficits, we examined the corner test and the cylinder test on the indicated time point after MCAO onset (detailed experimental methods have been described elsewhere[21]). Neurological score was calculated as (number of ipsilateral turns)/10 for the corner test and as (number of non-impaired forelimb contact – number of impaired forelimb contact) / (number of non-impaired forelimb contact + number of impaired forelimb contact + number of both contact) for the cylinder test. To evaluate the infarct volume and immunohistochemistry of ischemic brain tissue, mice were euthanized with deep sedation and then transcardially perfused with phosphate-buffered saline (PBS) followed by 4% paraformaldehyde. The removed forebrain was coronally sliced at 1 mm thickness and then embedded in paraffin. The infarct area was detected by microtubule-associated protein 2 (MAP2) staining and measured using ImageJ software (National Institutes of Health) in a blinded manner. To detect neuronal cell death in the infarct area, paraffin-embedded sections were examined by TUNEL staining. TUNEL-positive dead neuronal cells within three different 0.1 mm^2 areas were counted in the peri-infarct region

(considered to be expanded 2.0 to 2.5 mm lateral from the midline) as described previously.[19–21] To investigate the production of DAMPs, deparaffinized sections were stained using anti-PRX5 or anti-DJ-1 antibody, and then PRX5- or DJ-1-positive areas in TUNEL-positive regions were measured.[21]

METHOD DETAILS

Lipidomics analysis

Electrospray ionization tandem mass spectrometry (ESI-MS/MS) was performed as described previously.[66] In brief, to measure the amount of phospholipids in the brain tissue, collected brain tissue before or after MCAO was homogenized with 10 volumes of 50 mM Tris-HCl (pH 7.4), and then lipids were extracted from homogenates by the Bligh and Dyer method. To measure the amount of fatty acid and their oxygenated metabolites, the brain tissue was homogenized in 10 volumes of methanol and incubated at -20°C overnight. Then, water was added to the mixture at a final methanol concentration of 10% (v/v). This mixture was applied to Oasis HLB cartridges (Waters), washed with 10 mL of hexane, eluted with 3 mL of methyl formate, dried under N_2 gas, and dissolved in 60% methanol. The samples were applied to a Kinetex C18 column (2.1 mm i.d. × 150 mm length, 1.7 μm particle) (Phenomenex) coupled to ESI-MS/MS. Mass spectrometry analysis was performed using a 4000 QTRAP quadrupole-linear ion trap hybrid mass spectrometer (AB Sciex) with liquid chromatography (LC; NexeraX2 system; Shimadzu). The lipids were identified by multiple reaction monitoring (MRM) transition and retention times and quantified based on the peak area of the MRM transition. The calibration curve was obtained with an authentic standard for each compound. d5-labeled EPA (0.5 nmol; Cayman Chemicals) and LPC17:0 (0.5 nmol; Avanti Polar Lipids) were added to each sample as internal standards.

Microarray

Total RNA was extracted from the sham-operated or ischemic brain tissue and purified using a RNeasy Mini Kit (QIAGEN). The quality of RNA was assessed using a 2100 Bioanalyzer (Agilent Technologies). cDNA was synthesized with a Low Input QuickAmp Labeling Kit according to the manufacturer's protocol (Agilent Technologies). Samples were hybridized to a Whole Mouse Genome Microarray Kit (4 × 44K; Agilent Technologies), washed, and then scanned using a SureScan Microarray Scanner (Agilent Technologies). Microarray data were analyzed with Feature Extraction software (Agilent Technologies) and then imported into GeneSpring GX software (Agilent Technologies). Probes were normalized by quantile normalization among all microarray data.

Quantitative polymerase chain reaction (qPCR)

Total RNA was extracted from sham-operated or ischemic brain tissue using RNAiso (Takara). First-strand cDNA was synthesized using a High Capacity cDNA Reverse Transcriptase Kit (Applied Biosystems). Polymerase chain reactions were carried out using a SsoFast EvaGreen Supermixes (Bio-Rad) or TaqMan Gene Expression System (Applied Biosystems) on the CFX Connect (Bio-Rad).

Isolation of the immune cell-enriched population

Before or after MCAO, mice were transcardially perfused with PBS. The forebrain was removed and homogenized with RPMI-1640. After a final 1 mg ml^{-1} of collagenase (Sigma-Aldrich) and 50 μg ml^{-1} of DNase I (Roche) were added to the homogenates, brain homogenates were digested for 45 min and then subjected to Percoll (GE Healthcare) gradient centrifugation. From the interlayer between 37% and 70% Percoll, cells were isolated and stained with anti-CD45 FITC (11-0451-82, eBioscience), anti-CD11b PerCP-Cy5.5 (M1/70, eBioscience), anti-MSR1 (CD204) APC (MCA1322A647T, Bio-Rad), and anti-MARCO RPE (GTX39743, GeneTex). The cells were washed with PBS and analyzed by FACSAriaIII (BD). To examine mRNA expression levels, total RNA was purified using a ReliaPrep RNA Cell Miniprep System (Promega) and applied to qPCR analysis.

Isolation of neuronal cells from the adult brain

Neuronal cells were isolated from adult normal or ischemic brain according to the protocol established in the Allen Institute as described previously.[41] In detail, mice were deeply anesthetized with isoflurane and transcardially perfused with NMDG- artificial cerebrospinal fluid (NMDG-ACSF; 93 mM NMDG, 20 mM HEPES, 2.5 mM KCl, 30 mM NaHCO$_3$, 1.2 mM NaH$_2$PO$_4$, 0.5 mM CaCl$_2$, 10 mM MgCl$_2$, 25 mM glucose, 1 mM kynurenic acid, 0.2 mM Lidocaine HCl, 5 mM sodium ascorbate, 3 mM sodium pyruvate, 2 mM thiourea, pH 7.4). The forebrain was removed and soaked in NMDG-ACSF on ice. The removed forebrain was sliced at a 300 μm thickness and then incubated in NMDG-ACSF for 15 min at 34°C. The peri-infarct brain tissues that were considered to be expanded 2.5 mm lateral from the midline were cut out from the brain slices. The collected peri-infarct brain tissues were digested with pronase in HEPES-ACSF (92 mM NaCl, 20 mM HEPES, 2.5 mM KCl, 30 mM NaHCO$_3$, 1.2 mM NaH$_2$PO$_4$, 0.5 mM CaCl$_2$, 10 mM MgCl$_2$, 25 mM glucose, 1 mM kynurenic acid, 0.2 mM Lidocaine HCl, 5 mM sodium ascorbate, 3 mM sodium pyruvate, 2 mM thiourea, pH 7.4) bubbled with 95% O_2/5% CO_2 for 70 min. After a three-time wash with HEPES-ACSF containing 1% fetal bovine serum (FBS) and 0.2 % bovine serum albumin (BSA), digested peri-infarct brain tissues were triturated with fire-polished Pasteur pipettes. The dissociated brain cells containing neuronal cells were stained with anti-Thy1.2 PE (105307, BioLegend), anti-ACSA2 APC (130-116-142, Miltenyi Biotec), anti-CD31 PE-Cy7 (102523, BioLegend), anti-CD45 FITC (11-0451-82, eBioscience), anti-O4 APC (130-118-978, Miltenyi Biotec), anti-CD140a APC (135907, BioLegend), and anti-CD140b APC (136007, BioLegend), and analyzed by

FACS. The Thy1.2-positive and ACSA2-, CD31-, CD45-, O4-, CD140a-, and CD140b-negative population was isolated as the neuronal cell-enriched population. The purity of neuronal cells was confirmed using scRNA-seq or by *Vglut1-Cre*; Ai14 mice (Figure S2). SYTOX Green nucleic acid stain (S7020, Invitrogen) was additionally performed to remove dead neuronal cells for scRNA-seq analysis.

RNA-seq

Neuronal cell-enriched population isolated from the normal or peri-infarct brain tissue was pelleted for 5 min at 300×g at 4°C, and total RNA was purified using RNeasy Mini Kit (QIAGEN). RNA-seq libraries were prepared from total RNA using an Ovation SoLo RNA-Seq Library Preparation Kit (Tecan) according to the manufacturer's protocol. After the amount and fragment size distribution of obtained cDNA libraries were examined using an Agilent 2100 Bioanalyzer, the libraries were sequenced by Illumina HiSeq. Reads were mapped to mm10 (annotation file) by hisat2 after trimming adapter and low-quality sequences by Trimmomatic. The mapped reads were counted for each gene by featureCounts. Differentially expressed genes were analyzed by edgeR (glmQLFTest function). The integrated data of replicated samples from three independent experiments after the trimmed mean of M-values (TMM) normalization are shown by volcano plots. The genes whose expression levels were significantly increased or decreased in the comparison between two groups were further analyzed by gene ontology analysis performed with g:Profiler (version e104_eg51_p15_3922dba) with g:SCS multiple testing correction methods applying a significance threshold of 0.05. All genes expressed in neurons (CPM > 0) were used as the background gene set.

scRNA-seq

Two replicates of day 4 post-ischemic brain tissues of *Padi4*[flox/flox] and *Vglut1-Cre*; *Vgat-Cre*; *Padi4*[flox/flox] mice, as well as a single normal brain tissue of a sham-operated mouse, were sampled for scRNA-seq. Libraries of these five samples were prepared using Chromium Next GEM Single-cell 3′ Reagent Kits v3.1 (10x Genomics) according to the manufacturer's protocol. Neuronal cell-enriched population isolated by FACS was centrifuged for 10 min at 230×g at 4°C, and resuspended HEPES-ACSF containing 1% FBS and 1 % BSA. Single cells were loaded onto chromium chips with a capture target of 2,000 to 7,000 cells per sample. Libraries were sequenced on a DNBSEQ-G400 (MGI) with a targeted sequencing depth of more than 50,000 read pairs per cell. Read mapping and counting were processed with the 10x Genomics Cell Ranger 6.0.1[67] with the mm10 reference genome assembly and gene annotation provided by 10x Genomics. Sequencing statistics are shown in Table S6. Spliced-read counts for the individual genes were normalized by the SC Transformation method incorporated in Seurat 4.0.4.[68,69] The single-cell gene expression profiles of the five samples were merged by the Seurat anchor-based integration method.[70] This integrated count matrix was used to cluster the cells with the shared nearest-neighbor approach implemented in Seurat, resulting in their classification into 25 groups with a resolution value of 0.22. The clustering contained 14 groups consisting of glutamatergic neurons that were inferred based on the expression levels of *Snap25* and *Slc17a7*. Spliced and unspliced read counts were computed with the velocyto 0.17.17 package[71] from the BAM files generated by Cell Ranger. The ratio of spliced and unspliced read abundance for the individual cells were computed by total number of the reads of these two conditions in a cell. The UMAP plot of all cells of the five samples was generated with the Seurat Dimplot module by employing the normalized spliced read counts. From this plot, a subset of glutamatergic neurons was extracted. The visualization of the UMAP plot and differential expression analysis between cell populations were performed with the 10x Genomics Loupe Browser 6.0.0.

For the analysis of gene expression associated with recovery processes after brain injury, the total read counts of genes belonging to the ontologies listed in Data file S1 that were associated with nervous system reconstruction, synaptic organization, or remyelination were normalized and integrated by Seurat (819 recovery-process-associated genes were included from 3000 highly variable genes selected by the Seurat SelectIntegrationFeatures function). The total read counts of genes were averaged in each glutamatergic neuron cluster and were then shown in a bubble plot of Z-score for comparison among all of the obtained glutamatergic neuron clusters.

ATAC-seq

ATAC-seq library was prepared according to the protocol described elsewhere.[72] Briefly, neurons isolated from the brain tissue were pelleted for 15 min at 500×g at 4°C, lysed by cell lysis buffer (10 mM Tris-HCl, 10 mM NaCL, 3 mM MgCl2, 0.1 % IGEPAL CA-630) for 30 min at 500×g at 4°C, and treated with Tn5 transposase (Illumina, Nextera DNA Library Preparation Kit) for 60 min at 37°C for fragmentation and tagmentation of genome DNA. The DNA fragments were purified with SPRI select beads (BECKMAN), and PCR amplified with KAPA HiFi HS ReadyMix (KAPA BIOSYSTEMS) and Illumina dual index primers. The amplified DNA fragments were purified again with SPRI select beads . After the amount and fragment size distribution of obtained ATAC-seq libraries were examined using an Agilent 2100 Bioanalyzer, libraries were sequenced by Illumina HiSeq sequencer. Reads were mapped to mm10 (genome file) by Bowtie2 after removing adapter sequences by Trimmomatic. ATAC-seq signal peaks were detected by Genrich with ATAC-seq mode and default parameters. The correlation between the area under curve (AUC) of detected peaks within the genomic regions from the transcription start site -10 kb to the transcription end site +10 kb and the mRNA expression level (TPM) in RNA-seq was shown as a result.

CUT&Tag (Cleavage under targets and tagmentation)

The CUT&Tag library was prepared using a slightly modified Bench top CUT&Tag V.2 protocol described elsewhere (https://www.protocols.io/view/bench-top-cut-amp-tag-kqdg34qdpl25/v2). Immediately post-sorting, cells (12,000–14,000 cells) were pelleted for 3 min at 600×g at room temperature. Collected cells were resuspended in wash buffer (20 mM HEPES pH 7.5; 150 mM NaCl; 0.5 mM Spermidine; 1:100 Protease inhibitor cocktail; Nacalai Tesque) and mixed with activated concanavalin A-coated magnetic beads for 10 min at room temperature. Samples were placed on a magnet, the supernatant was removed, and 50 μL of ice-cold anti-body buffer (0.0025% digitonin; 20 mM HEPES pH 7.5; 150 mM NaCl; 0.5 mM spermidine; 1:100 protease inhibitor cocktail; 2 mM EDTA; 1% BSA) containing primary antibody (1:50 dilution, anti-histone H3 (citrulline R2+R8+R17) antibody: ab5103, Abcam) was added and incubated at 4°C overnight. The samples were placed on a magnet stand to clear, and the primary antibody buffer was removed. Wash buffer containing secondary antibody (1:100 dilution, guinea pig anti-rabbit IgG antibody: ABIN101961, antibodies-online.com) was added and gently shaken for 1 hour at room temperature with a shaker. After two washes with wash buffer, a 1:200 dilution of the pA-Tn5 adapter complex, which was prepared in Dig-325 buffer (0.025% digitonin, 20 mM HEPES, pH 7.5, 325 mM NaCl, 0.5 mM spermidine, 1:100 protease inhibitor cocktail), was added to the sample and then incubated with pA-Tn5 for 1 hour at room temperature. The samples were placed on a magnet stand to clear and washed three times with Dig-325 buffer. Tagmentation buffer (10 mM $MgCl_2$ in Dig-325 Buffer) was added and incubated at 37°C for 1 hour. To stop tagmentation and solubilize DNA fragments, 2.25 μL of 0.5 M EDTA, 2.75 μL of 10% SDS, and 0.5 μL of 20 mg/mL proteinase K were added to each sample, mixed at full-speed vortex for 2 seconds, and incubated at 50°C for 1 hour. For DNA purification, 122 μL of SPRI select beads was added to each sample, spun quickly, and held for 5 minutes. The tubes were placed on a magnetic stand to clear, the supernatant was discarded, the pellet was washed twice with 200 μL of 80% ethanol, and dried for 2 minutes. Then, 11 μL of TE (1 mM Tris-HCl pH 8.0, 0.1 mM EDTA) was added and allowed to stand for 5 minutes. The tube was placed on a magnetic stand, and the liquid was withdrawn to a fresh tube. For library amplification, 10.5 μL of DNA solution was mixed with 1 μL of i5 and i7 primers (10 mM) each with unique barcodes for each sample, followed by the addition of 12.5 μL of NEBNext HiFi 2× PCR Master Mix (New England BioLabs). Samples were placed in a thermocycler with a heated lid using the following cycling conditions: 72°C for 5 min, 98°C for 30 s; 18 cycles of [98°C 10 s, 63°C 30 s]; 72°C 1 min final extension, held at 4°C. Finally, 25 μL of Low-TE was added to the Post-PCR sample and 25 μL of SPRI select beads was added and incubated for 10 minutes. The supernatant was transferred to a new tube, and 15 μL of SPRI select beads was added. Samples were incubated for 10 min, washed twice with 80% ethanol, and eluted with 12 μL of 10 mM Tris pH 8.0. Sequencing was performed using the PE150 strategy (HiSeq 2500, Illumina). Reads were trimmed and mapped by the same process as ATAC-seq. Peak calling was performed by Genrich with normal mode and default parameters. ATAC-seq and CUT&Tag signals in histone H3 citrullination sites within the genomic regions from the transcription start site −10 kb to the transcription end site +10 kb were averaged and plotted by deepTools.

Padi4 luciferase reporter assay

Neuro-2a cells, a mouse neuroblastoma cell line, were cultured in DMEM (high glucose) (Nacalai Tesque, Cat#08459-64) containing 10% FBS (Sigma, Cat#173012), 1% penicillin-streptomycin (Nacalai Tesque, Cat#26253-84), and 1% 200 mM L-glutamine stock solution (Nacalai Tesque, Cat#16948-04) at a seeding density of 3.0×10^4 cells/well/24-well dish for 2 days. The 3 kb upstream promoter region from the transcription start site of the *Padi4* gene was PCR amplified (forward primer: AAAACGCGTAACAATGAGTGACCCTGCTTTAACAATGGGGGAGC; reverse primer: TTTTGTCGACGCCAGGCGAGCCCATGAGTCAGCACCT) from C57BL/6J mouse genome DNA, and cloned into the pGL3-Basic luciferase reporter vector (Promega). The transfection of the pGL3-Basic-Padi4-promoter-luciferase vector and the CMV-β-galactosidase vector (internal control) into Neuro-2a cells was conducted using a Viofectin transfection reagent (Viogene). Eighteen hours after the culture, each individual lipid listed below was added to the Neuro-2a cells. Twenty-four hours after the addition, the luciferase activity was measured by the luciferase assay system (Promega), relative to one of Neuro-2a cells without treatment. Palmitic acid (Sigma Aldrich, Cat#P9417), stearic acid (Sigma, Cat#S4651), palmitoleic acid (Sigma, Cat#P9417), oleic acid (Sigma, Cat#O1008), 5(Z),8(Z),11(Z)-eicosatrienoic acid (mead acid) (Cayman Chemical, Cat#90190), 5(S)-HETrE (Cayman Chemical, Cat#36230), α-linolenic acid (Sigma, Cat#L2378), 9(S)-HpOTrE (Cayman Chemical, Cat#45120), 13(S)-HpOTrE (Cayman Chemical, Cat#45220), 9(S)-HOTrE (Cayman Chemical, Cat#39420), 13(S)-HOTrE (Cayman Chemical, Cat#39620), 11(Z),14(Z),17(Z)-eicosatrienoic acid (DALA) (Cayman Chemical, Cat#90192), stearidonic acid (Sigma, Cat#SMB00291), eicosapentaenoic acid (EPA) (Sigma, Cat#E2011), docosapentaenoic acid (n-3 DPA) (Cayman Chemical, Cat#90165), docosahexaenoic acid (DHA) (Sigma, Cat#D2534), 6(Z),9(Z),12(Z),18(Z),21(Z)-tetracosahexaenoic acid (Cayman Chemical, Cat#10005165), linoleic acid (Sigma, Cat#L1376), 13(S)-HODE (Cayman Chemical, Cat#38610), γ-linolenic acid (GLA) (Sigma, Cat#L2378), 13(S)-HOTrE (γ) (Cayman Chemical, Cat#39610), prostaglandin E1 (Cayman Chemical, Cat#13010), 15-keto prostaglandin E1 (Cayman Chemical, Cat#13680), 13,14-dihydro-15-keto prostaglandin E1 (Cayman Chemical, Cat#13650), dihomo-γ-linolenic acid (DGLA) (Cayman Chemical, Cat#90230), 8(S)-HETrE (Cayman Chemical, Cat#36360), 12(S)-HETrE (Cayman Chemical, Cat#18483), 15(S)-HETrE (Cayman Chemical, Cat#36720), prostaglandin F1α (Cayman Chemical, Cat#15010), 13,14-dihydro-15-keto prostaglandin F1α (Cayman Chemical, Cat#15670), arachidonic acid (AA) (Sigma, Cat#A3611), 5(S)-HETE (Cayman Chemical, Cat#34230), 8(S)-HETE (Cayman Chemical, Cat#34360), 12(S)-HETE (Cayman Chemical, Cat#34570), 15(S)-HETE (Cayman Chemical, Cat#34720), Docosatetraenoic acid (Sigma, Cat#D3659), all-cis-4,7,10,13,16-docosapentaenoic acid (n-6 DPA) (Cayman Chemical, Cat#10008335), 16:0 Lyso PC (Avanti, Cat#855675), 18:0 Lyso PS (Avanti, Cat#858144), and 18:0 Lyso PE (Avanti, Cat#856715).

Lipid administration

A total of 1 mg of stearic acid (Sigma, Cat#S4651) dissolved in ethanol or DGLA (Cayman Chemical, Cat#90230) or vehicle (ethanol) was administered by oral gavage to MCAO mice every 24 h (24, 48, and 72 h) after stroke onset. The administration of 1 mg DGLA per day (similar amount to a daily standard therapeutic dose of EPA) was considered to be equivalent to a moderately DGLA-enriched diet, as described elsewhere.[73] A total of 600 ng of 15(S)-HETrE (Cayman Chemical, Cat#36720) or vehicle (ethanol) was dissolved in 150 μL of PBS, and was then administered intravenously to MCAO mice every 24 h (24, 48, and 72 h) after stroke onset. To investigate the signaling pathway for 15-HETrE to induce PADI4 expression, we intraperitoneally administered each 5 mg kg^{-1} of GW9662, SR16832, GW6471, Fatostatin, GSK2033, or 10 mg kg^{-1} of edaglitazone to MCAO mice every 24 h (24, 48, and 72 h) after stroke onset. (all lipid signaling inhibitors and agonists were purchased from Tocris Bioscience.)

Immunohistochemistry

The forebrain collected from MCAO mice was coronally sliced at 1 mm thickness and then embedded in paraffin. The thin-sliced sections were deparaffinized and incubated with proteinase K (20 μg ml^{-1}) or boiled in citrate buffer using a microwave oven. After blocking with Blocking One Histo (Nacalai Tesque), the sections were incubated with anti-PADI4 (GTX11395, GeneTex), PLA2G2E (ab204576, Abcam), GAD67 (MAB5406, Millipore), CaMKII (ab22609, Abcam), NeuN (MAB377, Millipore), SCF (sc-13126, Santa Cruz Biotechnology), GFRα-1 (sc-271546, Santa Cruz Biotechnology), BDNF (ab203573, Abcam), Nurr1 (Nr4a2) (N1404, ThermoFisher), or PPARγ (16643-1-AP, Proteintech) antibody overnight at 4°C. Secondary antibodies, anti-rabbit IgG antibody conjugated with Alexa Fluor 488 (A11070, Invitrogen) or Alexa Fluor 546 (A11071, Invitrogen), and anti-mouse IgG antibody conjugated with Alexa Fluor 488 (A11017, Invitrogen) or Alexa Fluor 546 (A11018, Invitrogen) were used for detection of the primary antibody. Images of the sections were captured using a fluorescence microscope (BZ-X710, Keyence) or a confocal laser microscope (LSM710, Carl Zeiss).

For the immunohistochemistry of the human stroke brain sample, the thin-sliced sections were deparaffinized and boiled in citrate buffer using a microwave oven. Then sections were incubated with TrueBlack (Biotium) to suppress autofluorescence. After blocking with Blocking One Histo (Nacalai Tesque), the sections were incubated with anti-PADI4 (GTX11395, GeneTex), PLA2G2E (ab204576, Abcam), or NeuN (MAB377, Millipore) antibody overnight at 4°C. Secondary antibodies, anti-rabbit IgG antibody conjugated with Alexa Fluor 488 (A11070, Invitrogen) and anti-mouse IgG antibody conjugated with Alexa Fluor 546 (A11018, Invitrogen) were used for detection of the primary antibody. After the treatment with TrueVIEW Autofluorescence Quenching Kit (Vector Laboratories), images of the sections were captured using a fluorescence microscope (BZ-X710, Keyence). PLA2G2E- or PADI4-positive neurons within three different 0.4 mm^2 areas were counted in the normal region or peri-infarct region. Control brain samples without ischemic stroke were also examined by immunohistochemistry.

MS imaging

Three days after MCAO, forebrains were isolated and quickly frozen with liquid nitrogen. Brain sections of 8 μm thickness made by a cryostat were mounted onto indium-tin-oxide-coated glass slides and subjected to imaging mass spectrometry measurement. Brain sections were sprayed with 9-aminoacridine matrix (10 mg/mL in 80% methanol), then installed into a matrix-assisted laser desorption/ionization (MALDI) ion trap mass spectrometer (MALDI LTQ XL, Thermo Scientific) equipped with a 60 Hz N$_2$ laser at 337 nm. The laser scan pitch was set at 70 μm, and the laser was irradiated 50 times for each pixel at a repetition rate of 20 Hz. Mass spectra were acquired in the negative-ion mode, and ion transition at m/z 321.2 >221.2 (mass window: 0.75 u) was used to detect specific signals of 15-HETrE (not detected from 5-HETrE, 8-HETrE, and 12-HETrE). ATP (m/z 506.0) or lysophosphatidylinositol (18:0) (m/z 599.3) was also detected to identify the peri-infarct surviving region around the infarct area or infarct region, respectively. After the imaging measurement, these brain sections were stained with hematoxylin-eosin to detect infarct and peri-infarct regions.

QUANTIFICATION AND STATISTICAL ANALYSIS

Data are displayed as minimum to maximum box-and-whisker plots or means ± the standard error of the mean (SEM). An unpaired Student's t-test or Mann–Whitney U test were used to analyze the differences between two groups. For analysis of the differences among three or more groups, statistical significance was determined by analysis of variance (ANOVA) followed by *post hoc* multiple comparison tests (Dunnett's test, Tukey's test, or Sidak test) or Kruskal-Wallis test followed by *post hoc* multiple comparison tests (Dunn's test). $p < 0.05$ was considered to represent a statistically significant difference. The statistical analysis results are reported in Data file S2.

Supplemental information

PLA2G2E-mediated lipid metabolism triggers

brain-autonomous neural repair

after ischemic stroke

Akari Nakamura, Seiichiro Sakai, Yoshitaka Taketomi, Jun Tsuyama, Yoshimi Miki, Yuichiro Hara, Nobutaka Arai, Yuki Sugiura, Hideya Kawaji, Makoto Murakami, and Takashi Shichita

PLA2G2E-mediated lipid metabolism triggers brain-autonomous neural repair after ischemic stroke

Akari Nakamura, Seiichiro Sakai, Yoshitaka Taketomi, Jun Tsuyama, Yoshimi Miki, Yuichiro Hara, Nobutaka Arai, Yuki Sugiura, Hideya Kawaji, Makoto Murakami, Takashi Shichita
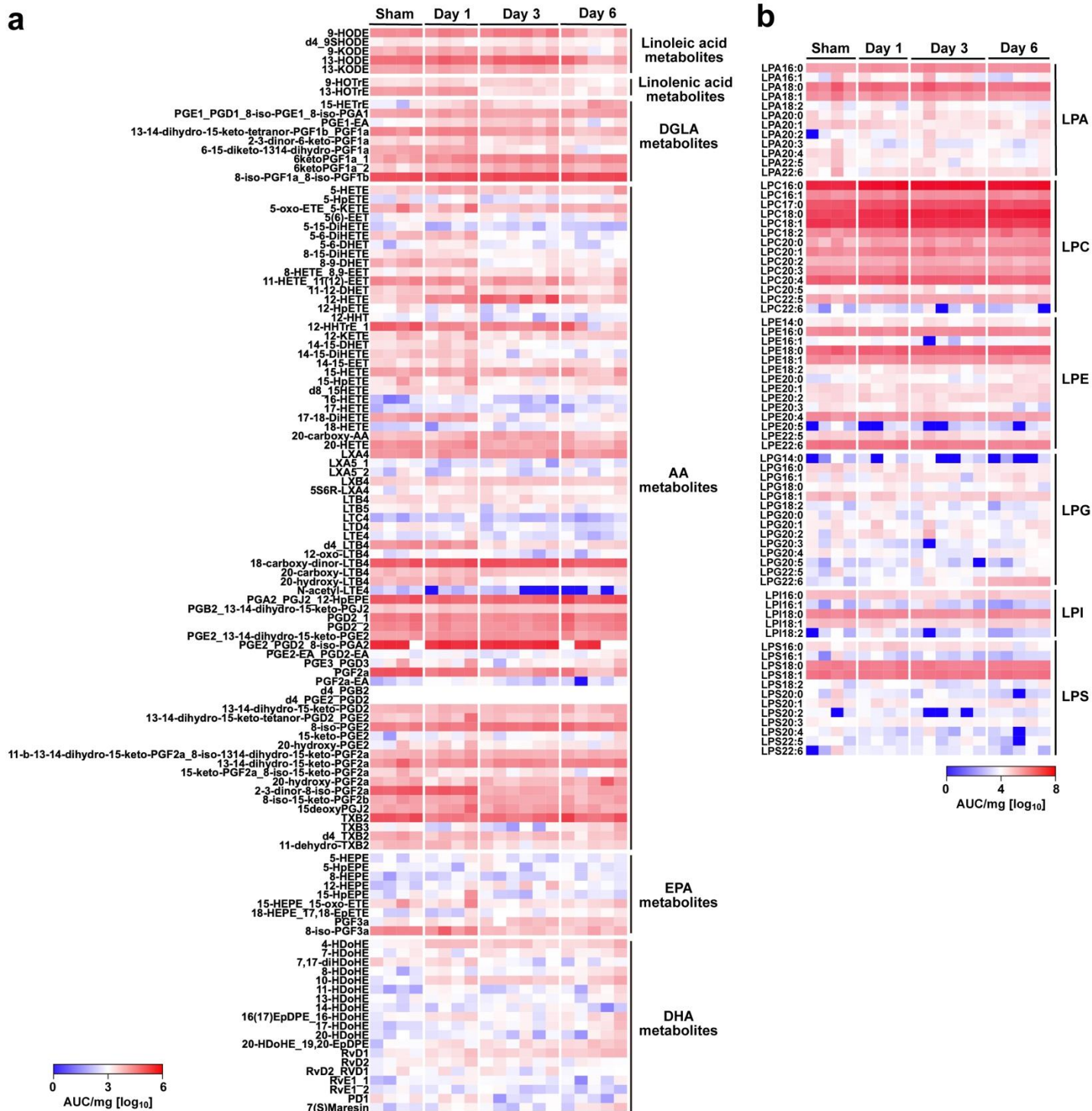
Figure S1. Actual values of lipid metabolite amounts in the brain tissue (related to Figure 1). Results of comprehensive mass spectrometry analysis of fatty acid metabolites (**a**) and lysophospholipids (**b**). Heatmaps showing the area under the curve (AUC) per 1 mg of each brain tissue.

2
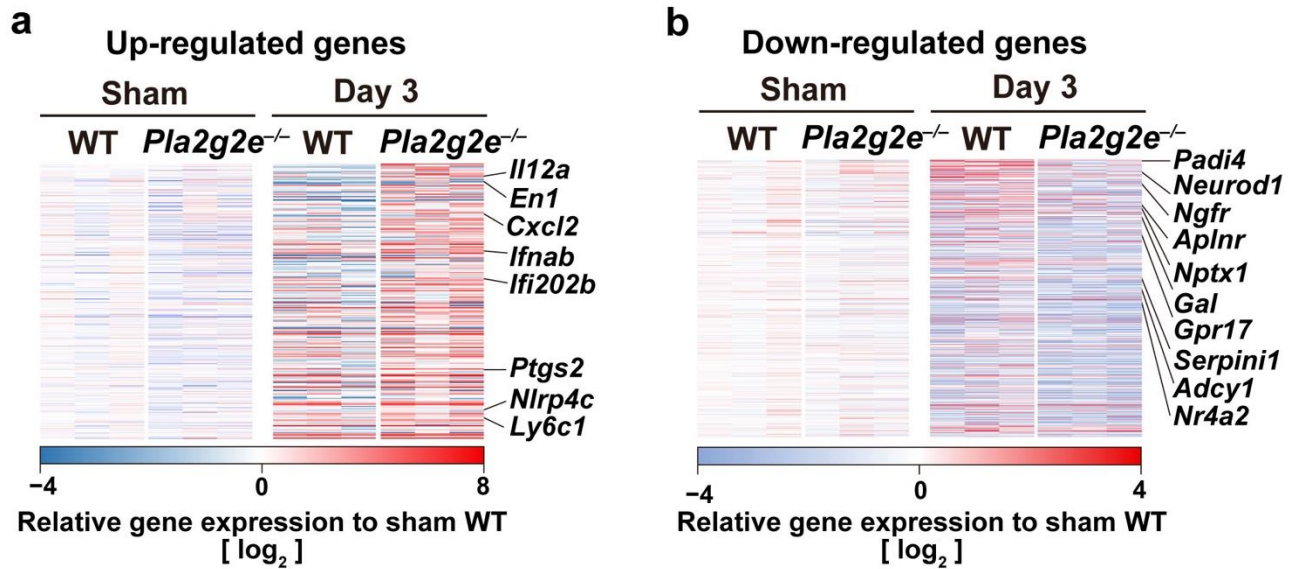
Figure S2. Results of microarray analysis in WT and *Pla2g2e*-deficient mice (related to Figure 2 and STAR Methods). (**a**,**b**) The comparison of mRNA expression levels in the genes whose expression levels were increased or decreased on day 3 after ischemic stroke onset between WT and *Pla2g2e*-deficient brain tissue. Day 3 data are the same as **Fig.2h** and **2j**.
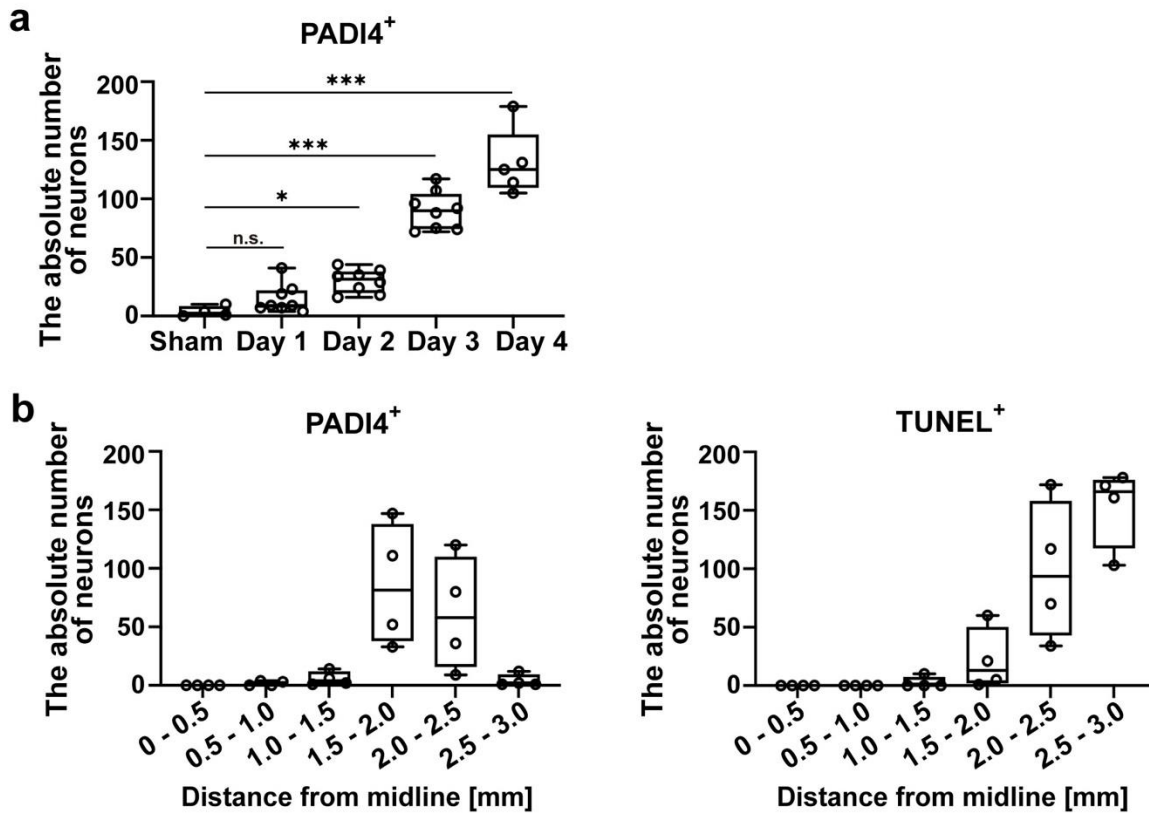
Figure S3. The number of each peri-infarct neuron detected by immunohistochemistry (related to Figure 3). (**a**) The absolute number of PADI4-positive neurons in the normal (sham-operated) or peri-infarct region (per 0.4 mm^2 areas at 2 mm far from midline) on each time point after ischemic stroke onset. (**b**) The absolute number of PADI4-positive neurons or TUNEL-positive dead neurons in the 0.4 mm^2 areas at each location distant from the midline on day 4 after ischemic stroke onset. *$p < 0.05$, ***$p < 0.001$ vs. sham-operated WT mice (**a**) (one-way ANOVA with Dunnett's correction). n.s.: not significant.
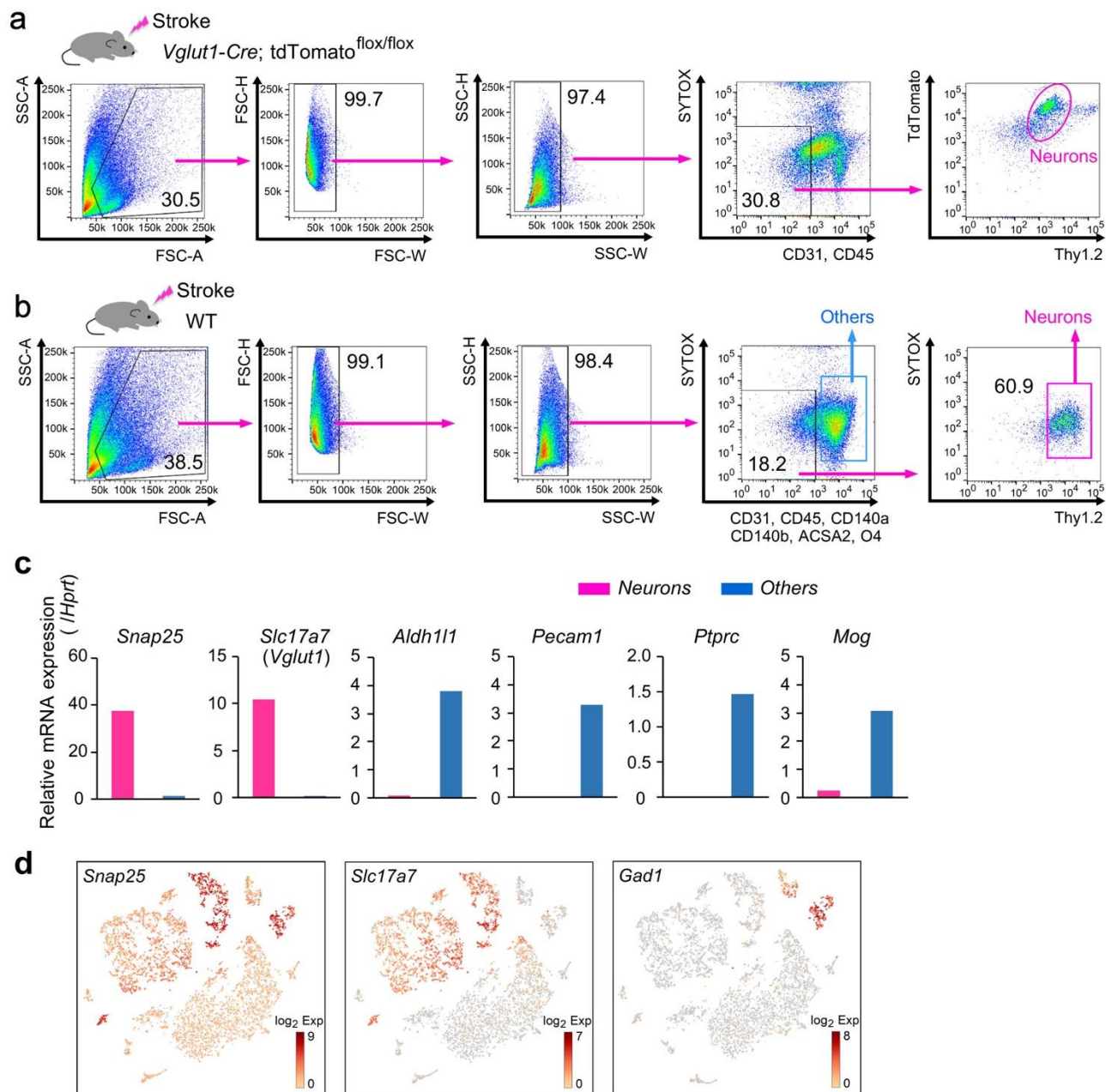
Figure S4. Sorting strategies of neurons collected from the ischemic brain (related to Figure 5). (**a**) The purity of neuronal populations isolated from peri-infarct surviving region of brain tissue was confirmed by using *Vglut1-Cre*; Ai14 (Rosa26-CAG-*loxP*-flanked STOP cassette-tdTomato) reporter mice. (**b**) Sorting strategy of neuronal cells for bulk RNA-seq or single-cell RNA-seq. (**c,d**) Isolation of neuronal cells was confirmed by quantitative PCR (**c**) or single-cell RNA-seq (**d**). *Snap25*: neuronal marker, *Slc17a7*: glutamatergic (excitatory) neuron marker, *Gad1*: GABAergic (inhibitory) neuron marker, *Aldh1l1*: astrocyte marker, *Pecam1*: endothelial cell marker, *Ptprc*: hematopoietic cell marker, *Mog*: oligodendrocyte marker. Cell distribution was shown by t-distributed stochastic neighbor embedding (tSNE) plot (**d**).
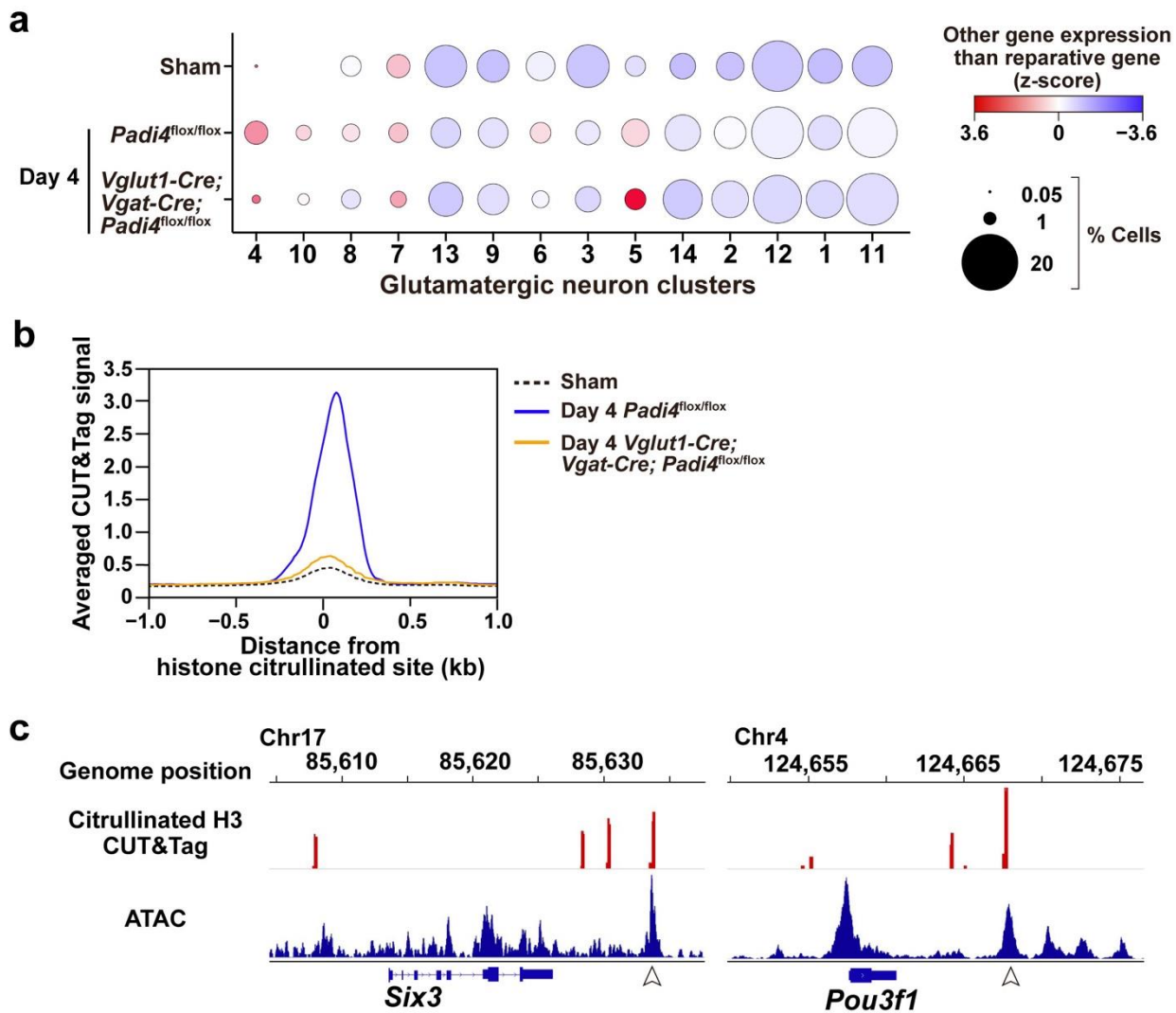
Figure S5. scRNA-Seq and epigenetic analysis of the peri-infarct neurons (related to Figure 5). (**a**) Bubble heatmap chart showing the read ratio of other genes than recovery-process-associated genes after brain injury. The size of the circles indicates the percentage of neurons that belong to each cluster. (**b**) The comparison of averaged histone-3-citrullination signal intensities around the histone-3-citrullinated sites in the day 4 peri-infarct neurons of *Padi4*flox/flox mice with ones in the neurons of sham-operated *Padi4*flox/flox or the day 4 peri-infarct neurons of *Vglut1-Cre*; *Vgat-Cre*; *Padi4*flox/flox mice in the same genomic regions. (**c**) Representative results of CUT&Tag analysis of citrullinated histone 3 (H3) and ATAC-seq analysis of recovery-process-associated gene (*Six3* and *Pou3f1*) loci in the neurons collected from day 4 peri-infarct regions of *Padi4*flox/flox mice. Blank arrowheads indicate the genome positions where the citrullinated H3 signal overlapped with the ATAC-seq signal.
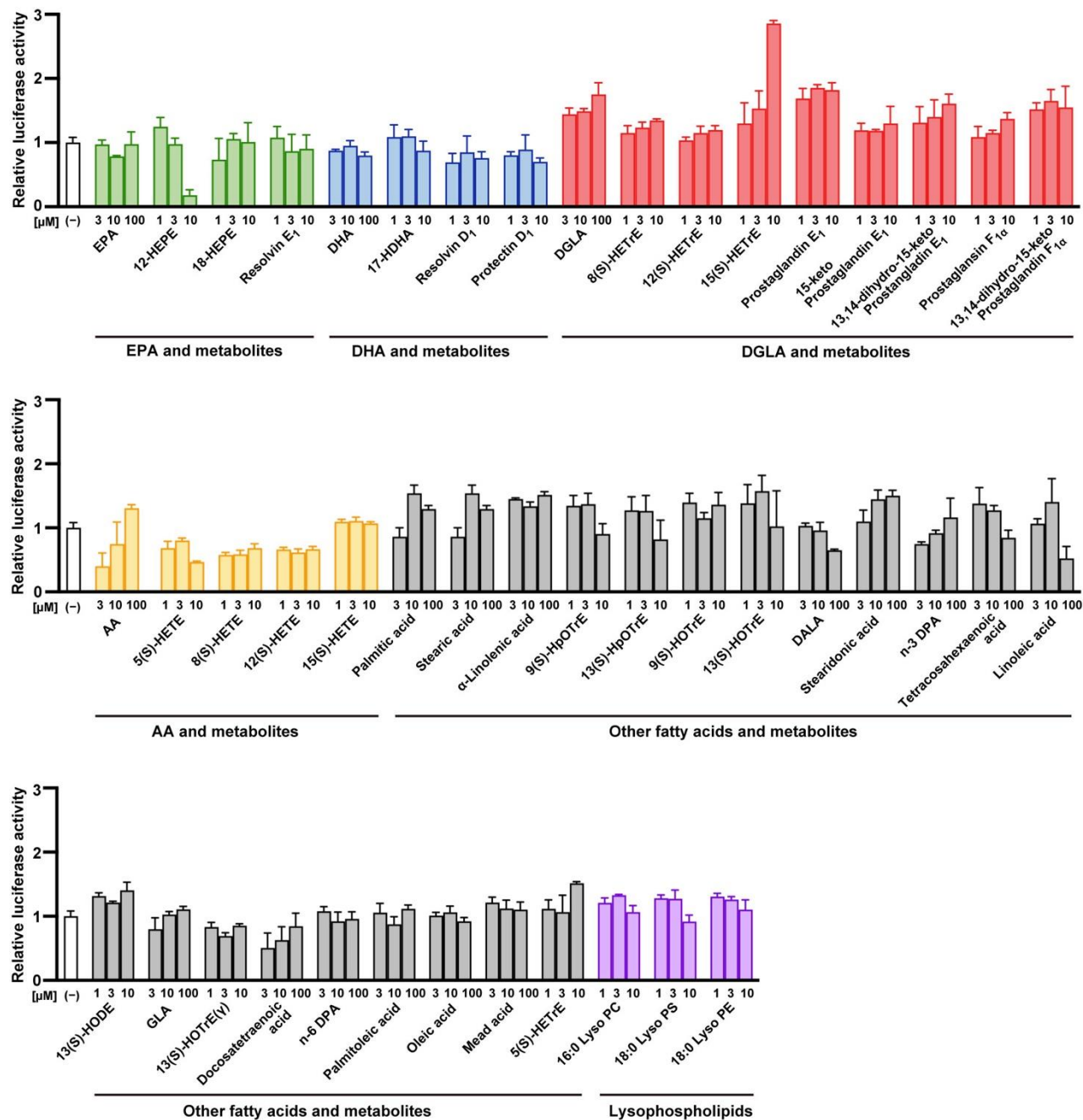
Figure S6. Measurements of the *Padi4*-inducing activity of each lipid metabolite (related to Figure 6). The luciferase-reporter activities under the *Padi4* gene promoter in the transfected Neuro-2a cells cultured with each lipid for 24 hours. The relative values were shown when compared to one of cells without treatment.
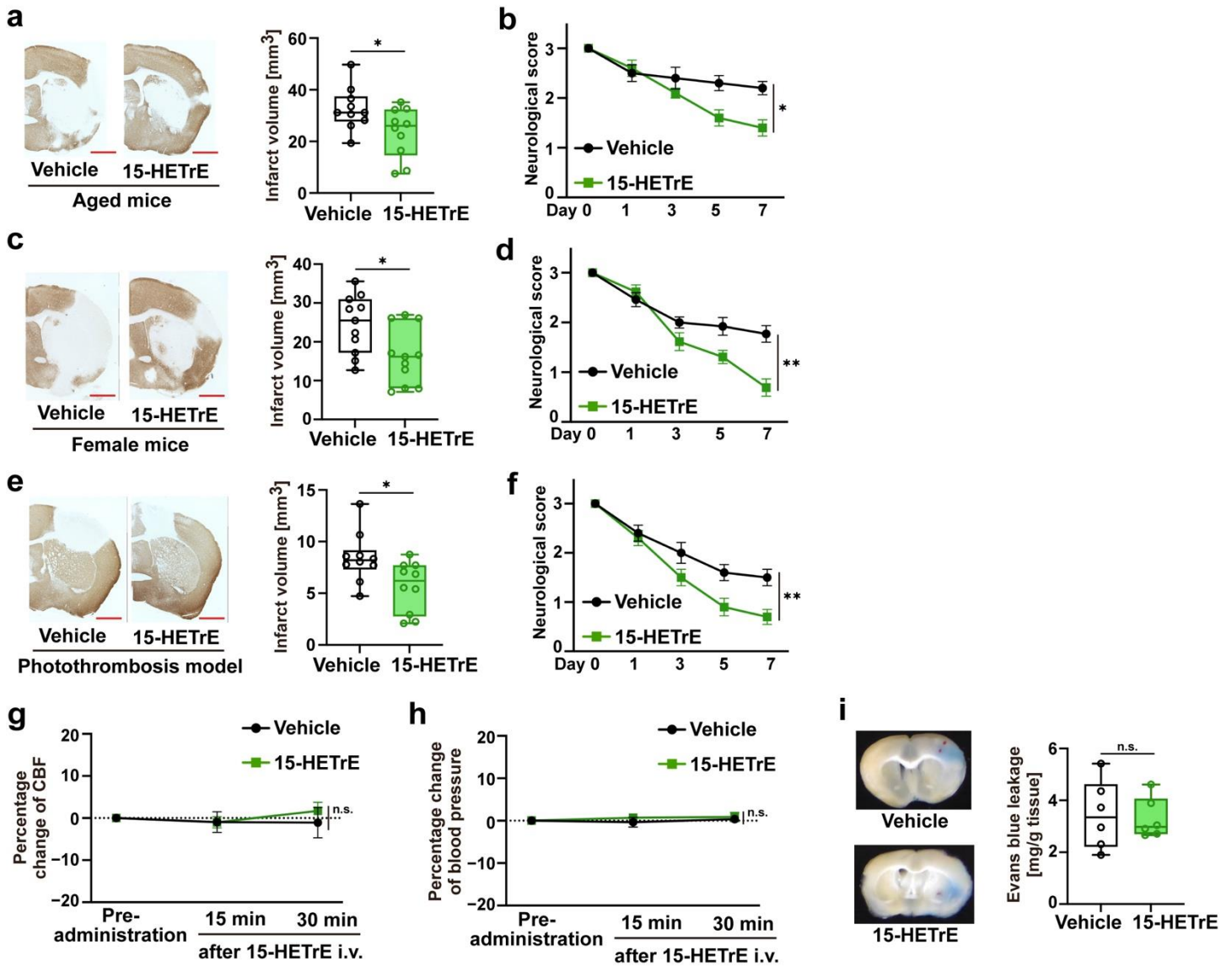
Figure S7. Therapeutic effects of 15-HETrE administration (related to Figure 7). (**a,b,c,d,e,f**) The comparison of infarct volume or neurological deficits between vehicle- and 15-HETrE-administered aged mice (**a,b**), female mice (**c,d**), and mice with photothrombotic stroke (**e,f**). (**g,h,i**) The changes in cerebral blood flow (CBF) (**g**), blood pressure (**h**), and the permeability of the blood-brain barrier (**i**) after the administration of vehicle or 15-HETrE to the mice 24 hours after ischemic stroke onset. *$p <$ 0.05, **$p <$ 0.01 vs. vehicle-administered mice (**a,b,c,d,e,f,g,h,i**) (two-sided Student's *t*-test [**a,c,e,i**] or two-way ANOVA [**b,d,f,g,h**]). n.s.: not significant. Error bars represent the mean ± standard error of the mean (SEM).
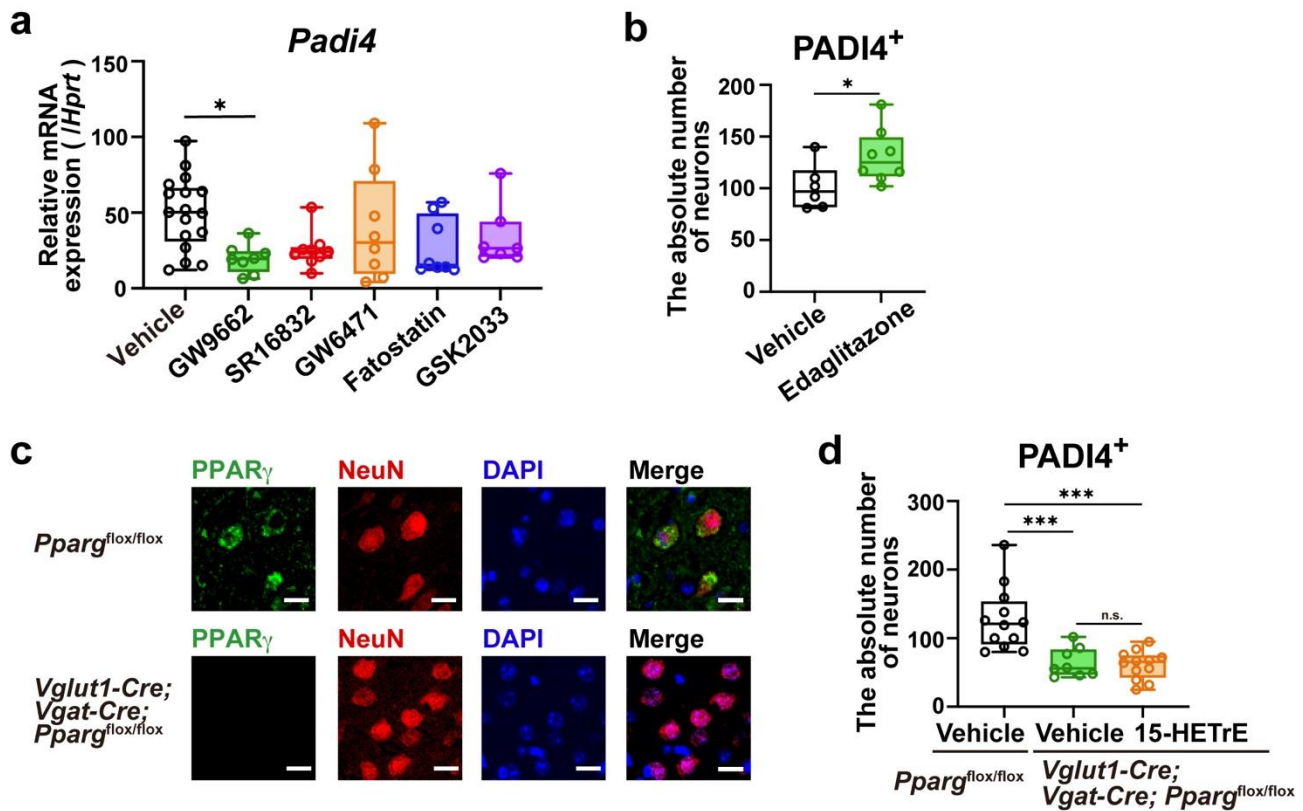
Figure S8. PPARγ-dependent induction of PADI4 in peri-infarct neurons (related to Figure 7). (**a**) The comparison of *Padi4* mRNA expression levels in day 3 post-ischemic brain tissue after the administration of each lipid-signal-inhibitor. GW9662 and SR16832: PPARγ antagonist, GW6471: PPARα antagonist, Fatostatin: inhibitor of sterol regulatory element binding protein (SREBP), GSK2033: LXR antagonist. (**b**) The absolute number of PADI4-positive neurons in the day 4 peri-infarct region of vehicle- or edaglitazone-administered mice. (**c**) The immunohistochemistry of PPARγ in the day 4 peri-infarct neurons of *Pparg*flox/flox and *Vglut1-Cre*; *Vgat-Cre*; *Pparg*flox/flox mice. Scale bar: 10 μm. (**d**) The absolute number of PADI4-positive neurons in the day 4 peri-infarct region of vehicle-administered *Pparg*flox/flox mice, vehicle- or 15-HETrE-administered *Vglut1-Cre*; *Vgat-Cre*; *Pparg*flox/flox mice). *$p < 0.05$, **$p < 0.01$, ***$p < 0.001$ vs. vehicle-administered WT mice (**a**,**b**), vehicle-administered *Pparg*flox/flox mice (**c**) (Kruskal-Wallis test with Dunn's test [**a**], two-sided Student's *t*-test [**b**], one-way ANOVA with Tukey's correction [**c**]). n.s.: not significant.

a

	WT	*Pla2g2e*$^{-/-}$	*Pla2g4e*$^{-/-}$	*Pla2g5*$^{-/-}$	*Pla2g10*$^{-/-}$	*Pla2g12a*$^{-/-}$
MABP (mmHg)	94 ± 5	95 ± 4	91 ± 2	92 ± 1	95 ± 2	94 ± 3
pH	7.40 ± 0.02	7.41 ± 0.02	7.39 ± 0.03	7.38 ± 0.01	7.40 ± 0.01	7.42 ± 0.01
PaO$_2$ (mmHg)	124 ± 9	124 ± 7	132 ± 7	124 ± 7	129 ± 4	123 ± 7
PaCO$_2$ (mmHg)	36.8 ± 1.3	37.2 ± 1.4	36.0 ± 1.6	37.7 ± 3.4	38.9 ± 1.3	37.6 ± 2.3
Hematocrit (%)	36 ± 1	40 ± 1	40 ± 2	38 ± 1	40 ± 0	41 ± 2
Glucose (mg/dl)	152 ± 9	143 ± 11	162 ± 12	137 ± 18	146 ± 4	138 ± 10

b

CBF reduction (%)	before CCA occlusion	after CCA occlusion	after MCA occlusion	N	Exclusion (N) Death	Exclusion (N) CBF	Survival rate (%) Day 4	Survival rate (%) Day 7
WT	100	80.4 ± 2.6	31.0 ± 1.8	20	0	1	90.0	70.0
Pla2g2e$^{-/-}$	100	82.5 ± 2.5	31.0 ± 1.4	24	0	1	87.5	58.3
Pla2g4e$^{-/-}$	100	83.9 ± 2.0	29.9 ± 1.1	16	0	0	93.8	87.5
Pla2g5$^{-/-}$	100	84.5 ± 2.2	30.0 ± 1.9	15	0	0	93.3	80.0
Pla2g10$^{-/-}$	100	82.4 ± 2.0	30.1 ± 0.9	10	0	0	90.0	80.0
Pla2g12a$^{-/-}$	100	79.8 ± 2.1	27.3 ± 2.0	17	1	0	94.1	76.5

c

WT   *Pla2g2e*$^{-/-}$ *Pla2g4e*$^{-/-}$ *Pla2g5*$^{-/-}$ *Pla2g10*$^{-/-}$ *Pla2g12a*$^{-/-}$

d

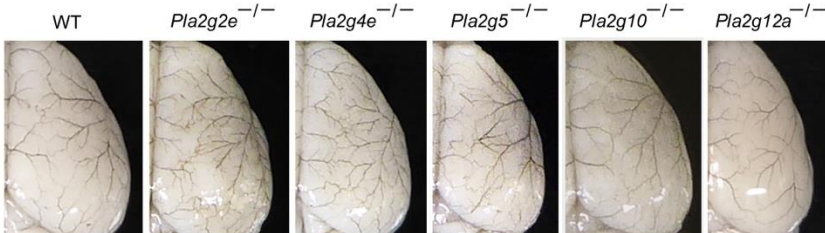|	WT	*Pla2g2e*$^{-/-}$	*Pla2g4e*$^{-/-}$	*Pla2g5*$^{-/-}$	*Pla2g10*$^{-/-}$	*Pla2g12a*$^{-/-}$
Number of anastomosis	8.5 ± 0.6	8.0 ± 0.4	8.5 ± 0.5	9.0 ± 1.1	9.0 ± 0.8	8.0 ± 0.6
Diameter of anastomosis (μm)	63 ± 4	62 ± 3	63 ± 7	67 ± 3	62 ± 4	63 ± 3
Diameter of ACA (μm)	130 ± 7	135 ± 9	138 ± 9	135 ± 13	130 ± 4	135 ± 5
Diameter of MCA (μm)	148 ± 3	145 ± 6	145 ± 6	143 ± 5	145 ± 6	150 ± 8
Diameter of PCA (μm)	143 ± 8	145 ± 6	143 ± 13	145 ± 3	148 ± 3	150 ± 9
Diameter of P-com (μm)	105 ± 5	108 ± 5	103 ± 6	105 ± 6	103 ± 5	105 ± 3

Table S1. Assessment of cerebral blood flow and vascular anatomy in WT and PLA2-subtype-deficient mice (related to Figure 2). (**a**) Physiological data from WT or each PLA2-subtype-deficient mice. (**b**) Changes in cerebral blood flow before and after the induction of brain ischemia, and the survival rate on day 4 and day 7 after stroke onset. There were no significant differences in physiological data and CBF between WT and each PLA2-subtype-deficient mice. Number of mice excluded upon death or non-satisfactory reduction of cerebral blood flow (CBF) during ischemia was shown. (**c**) Images of vascular structure in each mouse strain. (**d**) Measurements of the diameter of each cerebral artery composing the circle of Willis. The number and diameter of the leptomeningeal anastomosis of each mouse strain were also shown. There was no significant difference in each parameter among strains.

a

	Padi4 f/f	Vglut1-Cre; Vgat-Cre; Padi4 f/f	LysM-Cre; Padi4 f/f
MABP (mmHg)	92 ± 3	91 ± 4	88 ± 3
pH	7.41 ± 0.02	7.41 ± 0.01	7.40 ± 0.01
PaO_2 (mmHg)	139 ± 10	150 ± 7	149 ± 4
$PaCO_2$ (mmHg)	35.9 ± 2.4	37.1 ± 2.8	37.9 ± 1.8
Hematocrit (%)	37 ± 2	39 ± 2	38 ± 1
Glucose (mg/dl)	158 ± 10	158 ± 19	160 ± 13

b

CBF reduction (%)	before CCA occlusion	after CCA occlusion	after MCA occlusion	N	Exclusion (N) Death	Exclusion (N) CBF
Padi4 f/f	100	79.1 ± 2.5	29.7 ± 1.2	11	0	0
Vglut1-Cre; Vgat-Cre; Padi4 f/f	100	85.8 ± 2.2	29.3 ± 1.2	13	0	0
LysM-Cre; Padi4 f/f	100	83.4 ± 2.4	28.7 ± 1.5	11	0	0

c

Legend:
- Padi4 f/f
- Vglut1-Cre; Vgat-Cre; Padi4 f/f
- LysM-Cre; Padi4 f/f

d

Padi4 f/f | Vglut1-Cre; Vgat-Cre; Padi4 f/f | LysM-Cre; Padi4 f/f

e

	Padi4 f/f	Vglut1-Cre; Vgat-Cre; Padi4 f/f	LysM-Cre; Padi4 f/f
Number of anastomosis	8.3 ± 0.8	8.8 ± 0.8	7.8 ± 0.9
Diameter of anastomosis (μm)	62 ± 4	62 ± 5	65 ± 4
Diameter of ACA (μm)	135 ± 6	128 ± 8	128 ± 9
Diameter of MCA (μm)	145 ± 5	145 ± 6	150 ± 6
Diameter of PCA (μm)	145 ± 6	140 ± 7	140 ± 8
Diameter of P-com (μm)	110 ± 4	110 ± 9	105 ± 5

Table S2. Assessment of cerebral blood flow and vascular anatomy in *Padi4*flox/flox mice (related to Figure 3). (**a**) Physiological data from each *Padi4*flox/flox mice. (**b,c**) Changes in cerebral blood flow before and after the induction of brain ischemia (**b**), and the survival rate after stroke onset (**c**). Number of mice excluded upon death or non-satisfactory reduction of CBF during ischemia was shown. (**d**) Images of vascular structure in each mouse strain. (**e**) Measurements of the diameter of each cerebral artery composing the circle of Willis. The number and diameter of the leptomeningeal anastomosis of each mouse strain were also shown. There was no significant difference in each parameter among strains.
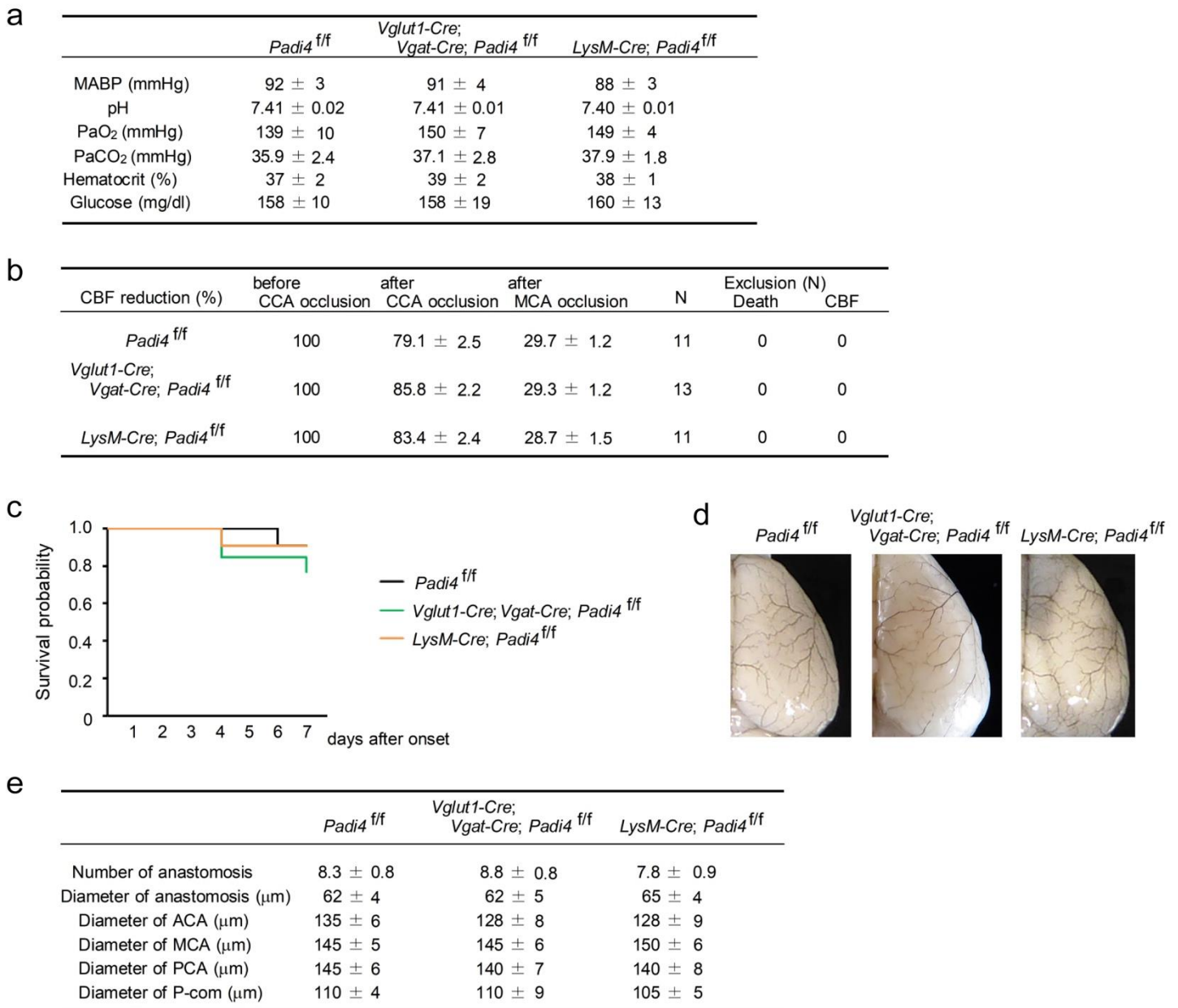
No.	Age/sex	Etiology, region of brain infarction	Cause of death	Comorbidities	tPA administration
1	78 Female	Atherothrombotic, left ACA, MCA, PCA territory (acute ICA occlusion, atherosclerosis)	Respiratory arrest due to cerebral herniation	Hypertension, Sick sinus syndrome	Not performed
2	78 Female	Cardioembolic, right ACA, MCA territory	Respiratory arrest due to cerebral herniation	Atrial fibrillation, Hypertrophic cardiomyopathy, Congestive heart failure	Not performed
3	71 Male	Cardioembolic, right ACA, MCA, PCA territory	Respiratory arrest due to cerebral herniation	Atrial fibrillation, Congestive heart failure	Not performed
4	55 Male	Atherothrombotic, left MCA territory (MCA origin occlusion)	Respiratory arrest due to cerebral herniation	Hypertension	Not performed
5	74 Male	Atherothrombotic, right ACA, MCA, PCA territory (acute ICA occlusion, atherosclerosis)	Respiratory arrest due to cerebral herniation	Diabetes mellitus, Arteriosclerosis obliterans	Not performed
6	70 Female	Embolic, left MCA territory (MCA origin occlusion, no significant atherosclerosis)	Respiratory arrest due to cerebral herniation	Cardiac hypertrophy, after closure of atrial septum defect, Syncope	Not performed
7	74 Female	Cardioembolic, right ACA, MCA territory	Respiratory arrest due to cerebral herniation	Atrial fibrillation, Hyperthyroidism	Not performed
8	80 Female	Embolic, left MCA territory (MCA origin occlusion, no significant atherosclerosis)	Rupture of aortic dissecting aneurysm	Hypertension, Congestive heart failure	Not performed

Abbreviations:
ACA: anterior cerebral artery, MCA: middle cerebral artery, PCA: posterior cerebral artery, ICA: internal carotid artery

Table S3. Detailed clinical information on ischemic stroke patients (related to Figure 4 and STAR Methods).

a

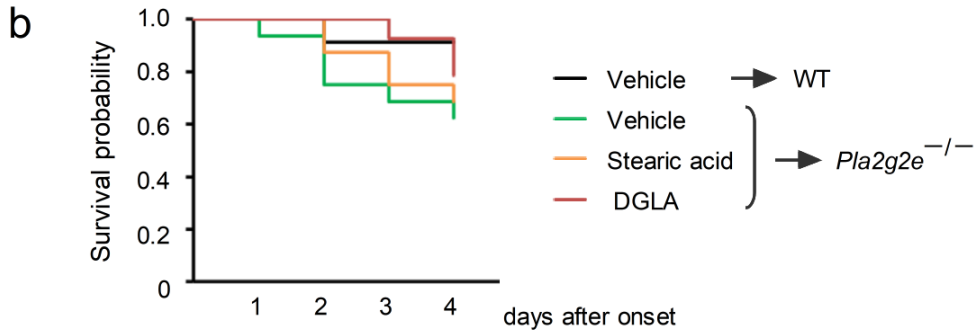| CBF reduction (%)		before CCA occlusion	after CCA occlusion	after MCA occlusion	N	Exclusion (N) Death	CBF
WT	Vehicle	100	84.1 ± 2.1	32.9 ± 0.9	12	0	0
$Pla2g2e^{-/-}$	Vehicle	100	82.0 ± 2.2	29.5 ± 1.4	16	0	0
	Stearic acid	100	85.2 ± 3.0	32.2 ± 1.5	14	0	0
	DGLA	100	86.0 ± 2.1	28.7 ± 1.6	16	0	0

b

Table S4. Results of cerebral blood flow and survival in the vehicle- or lipid-administered WT and *Pla2g2e*-deficient mice (related to Figure 6). Changes in cerebral blood flow before and after the induction of brain ischemia (**a**) and the survival rate after stroke onset (**b**). The number of mice excluded upon death or non-satisfactory reduction of CBF during ischemia was shown.

a

CBF reduction (%)		before CCA occlusion	after CCA occlusion	after MCA occlusion	N	Exclusion (N) Death	CBF
WT	Vehicle	100	86.9 ± 2.0	32.6 ± 1.0	13	0	0
	15-HETrE	100	85.5 ± 1.9	28.2 ± 1.6	12	0	0

b

c

d

CBF reduction (%)		before CCA occlusion	after CCA occlusion	after MCA occlusion	N	Exclusion (N) Death	CBF
Vglut1-Cre; Vgat-Cre; Padi4 f/f	Vehicle	100	85.4 ± 2.5	32.4 ± 1.2	13	0	0
	15-HETrE	100	88.2 ± 1.7	31.1 ± 1.1	14	0	0

e

f

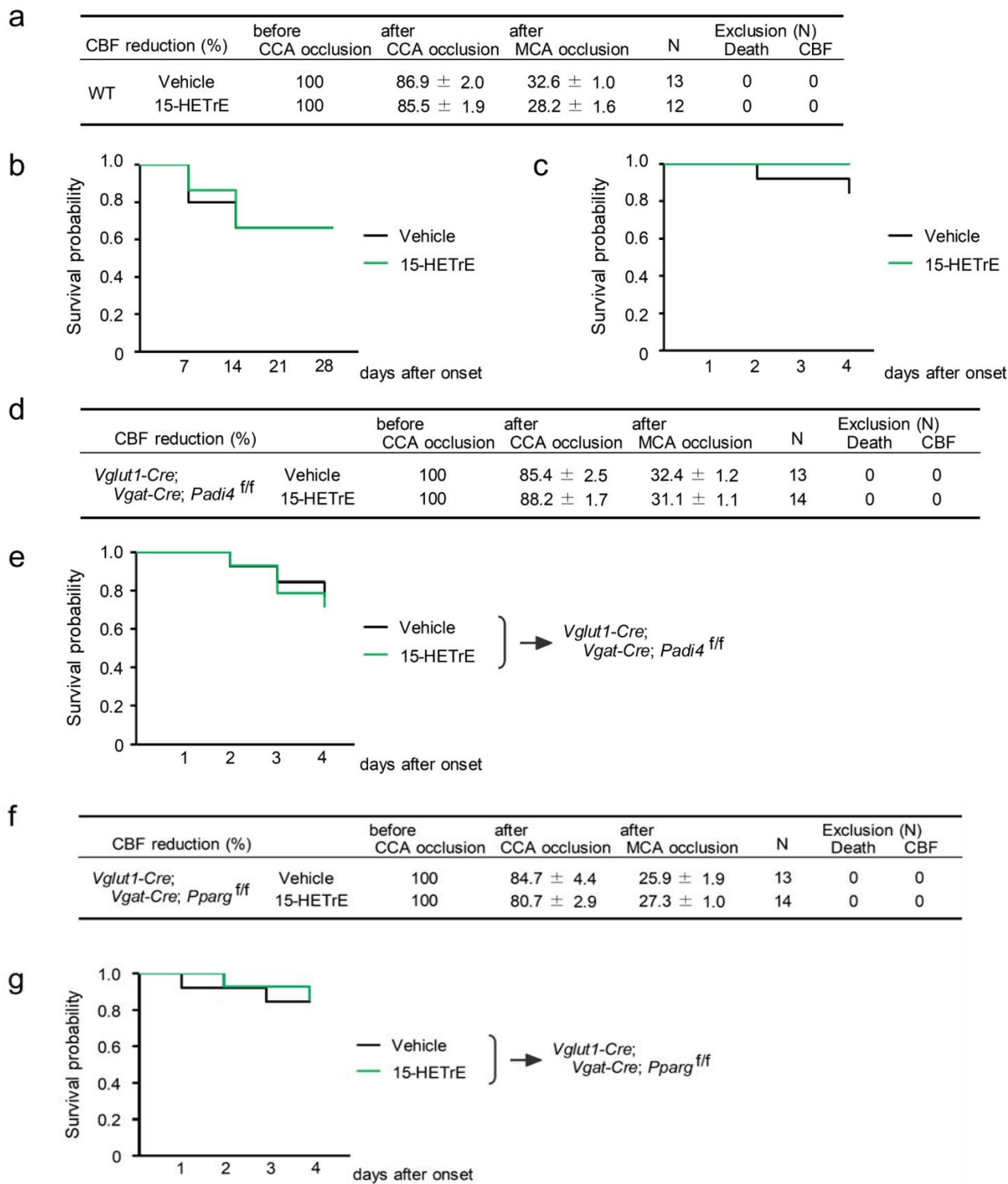| CBF reduction (%)		before CCA occlusion	after CCA occlusion	after MCA occlusion	N	Exclusion (N) Death	CBF
Vglut1-Cre; Vgat-Cre; Pparg f/f	Vehicle	100	84.7 ± 4.4	25.9 ± 1.9	13	0	0
	15-HETrE	100	80.7 ± 2.9	27.3 ± 1.0	14	0	0

g

Table S5. Results of cerebral blood flow and survival in vehicle- or 15-HETrE-administered mice (related to Figure 7). Changes in cerebral blood flow before and after the induction of brain ischemia (**a,d**), and the survival rate after stroke onset (**b,c,e**). The number of mice excluded upon death or non-satisfactory reduction of CBF during ischemia was shown.

Sample name	Estimated number of cells	Mean reads per cell	Median genes per cell
Sham	4,623	82,842	2,272
Day 4 *Padi4*^{flox/flox} - 1	5,807	62,765	2,815
Day 4 *Padi4*^{flox/flox} - 2	1,219	328,526	2,075
Day 4 *Vglut1-Cre; Vgat-Cre; Padi4*^{flox/flox} - 1	5,245	71,141	2,857
Day 4 *Vglut1-Cre; Vgat-Cre; Padi4*^{flox/flox} - 2	5,781	67,650	1,694

Table S6. Sequence result of single-cell RNA-seq of neuronal populations isolated from sham-operated brain or peri-infarct surviving region of brain tissue (related to Figure 5 and STAR Methods).

Mouse *Hprt1* forward primer	5'-TGAAGAGCTACTGTAATGATCAGTC-3'
Mouse *Hprt1* reverse primer	5'-AGCAAGCTTGCAACCTTAACCA-3'
Mouse *Tnf* forward primer	5'-CATCTTCTCAAAATTCGAGTGACAA-3'
Mouse *Tnf* reverse primer	5'-TGGGAGTAGACAAGGTACAACCC-3'
Mouse *Il1b* forward primer	5'-CAGGCAGGCAGTATCACTCA-3'
Mouse *Il1b* reverse primer	5'-AGGCCACAGGTATTTTGTCG-3'
Mouse *Il23a* forward primer	5'-AGCGGGACATATGAATCTACTAAGAGA-3'
Mouse *Il23a* reverse primer	5'-GTCCTAGTAGGGAGGTGTGAAGTTG-3'
Mouse *Padi4* forward primer	5'-GACCAATGGATGCAGGACG-3'
Mouse *Padi4* reverse primer	5'-AATCCTTCAGGCCTCTGTCC-3'

Table S7. The sequences of oligonucleotides used in qPCR, Related to STAR Methods